

“TNOs are Cool”: A survey of the trans-Neptunian region. XI. A Herschel-PACS^{*} view of 16 Centaurs

R. Duffard¹, N. Pinilla-Alonso^{1,2}, P. Santos-Sanz¹, E. Vilenius³, J.L. Ortiz¹, T. Mueller³, S. Fornasier⁴, E. Lellouch⁴,
M. Mommert⁵, A. Pal⁶, C. Kiss⁶, M. Mueller⁷, J. Stansberry⁸, A. Delsanti⁹, N. Peixinho¹⁰, and D. Trilling¹¹

¹ Instituto de Astrofísica de Andalucía - CSIC, Glorieta de la Astronomía s/n, Granada, Spain.
e-mail: duffard@iaa.es

² Department of Earth and Planetary Sciences, University of Tennessee, 1412 Circle Dr, Knoxville TN 37996-1410, USA.

³ Max-Planck-Institut für extraterrestrische Physik, Postfach 1312, Giessenbachstr., 85741 Garching, Germany.

⁴ LESIA-Observatoire de Paris, CNRS, UPMC Univ. Paris 6, Univ. Paris-Diderot, 5 place J. Janssen, 92195 Meudon Cedex, France

⁵ Deutsches Zentrum für Luft- und Raumfahrt e.V., Institute of Planetary Research, Rutherfordstr. 2, 12489 Berlin, Germany

⁶ Konkoly Observatory, Research Centre for Astronomy and Earth Sciences, Konkoly Thege 15-17, H-1121 Budapest, Hungary

⁷ SRON, Netherlands Institute for Space Research, Low Energy Astrophysics, Groningen, Netherlands.

⁸ Space Telescope Science Institute, 3700 San Martin Drive, Baltimore MD 21218, USA.

⁹ Laboratoire d'Astrophysique de Marseille, CNRS & Université de Provence, 38 rue Frédéric Joliot-Curie, 13388 Marseille Cedex 13, France

¹⁰ Unidad de Astronomía, Fac. de Ciencias Básicas, Universidad de Antofagasta, Avda. U. de Antofagasta 02800, Antofagasta, Chile.

¹¹ Department of Physics and Astronomy, Northern Arizona University, Flagstaff, AZ 86001, USA.

Received ; accepted

ABSTRACT

Context. Centaurs are the transitional population between trans-Neptunian objects (TNOs) and Jupiter-family comets. Their physical properties provide an insight into TNO properties, but only under restricted conditions since Centaurs are closer to the Sun and Earth. For this reason it is possible to access the smaller ones, which is more difficult to do with the TNO population.

Aims. The goal of this work is to characterize a set of 16 Centaurs in terms of their size, albedo, and thermal properties. We study the correlations, for a more extended sample obtained from the literature, of diameter, albedo, orbital parameters, and spectral slopes.

Methods. We performed three-band photometric observations using Herschel-PACS and used a consistent method for the data reduction and aperture photometry of this sample to obtain monochromatic flux densities at 70, 100, and 160 μm . Additionally, we used Spitzer-MIPS flux densities at 24 and 70 μm when available. We also included in our Centaur sample scattered disk objects (SDOs), a dynamical family of TNOs, using results previously published by our team, and some Centaurs observed only with the Spitzer/MIPS instrument.

Results. We have determined new radiometric sizes and albedos of 16 Centaurs. The first conclusion is that the albedos of Centaur objects are not correlated with their orbital parameters. Similarly, there is no correlation between diameter and orbital parameters. Most of the objects in our sample are dark ($p_v < 7\%$) and most of them are small ($D < 120\text{km}$). However, there is no correlation between albedo and diameter, in particular for the group of the small objects as albedo values are homogeneously distributed between 4 to 16%. The correlation with the color of the objects showed that red objects are all small (mean diameter 65 km), while the gray ones span a wide range of sizes (mean diameter 120 km). Moreover, the gray objects tend to be darker, with a mean albedo of 5.6%, compared with a mean of 8.5% (ranging from 5 to 15%) for the red objects.

Key words. Kuiper Belt: general.

1. Introduction

One fundamental question in astrophysics is how planetary systems form and evolve. Accurate physical properties of small solar system bodies are crucial pieces of information needed to understand the formation processes, and they constrain models of planetary formation and evolution. Centaurs are a dynamical class of small bodies in our solar system with orbits mostly in the region between Jupiter and Neptune that cross the orbits of one or more of the giant planets.

The first Centaur was discovered in 1977 and was named Chiron (who is the son of Kronos and grandson of Uranus in Greek mythology). It was the first minor planet with a perihelion distance far beyond Jupiter's orbit (Pluto was classified as a planet at that time). At least two objects were discovered earlier but were only re-classified as Centaurs after the discovery of Chiron. The next Centaur, Pholus, was discovered only 15 years later. Currently, there are 211 Centaurs listed by the Minor Planet Center (MPC) as of early February 2013 (URL:<http://www.minorplanetcenter.net/iau/lists/Centaurs.html>). A considerable fraction of them have been discovered only recently, since the beginning of 2010. We note that the MPC list includes scattered-disk objects (SDOs), but that some of those are considered to be Centaurs by some authors.

* Herschel is an ESA space observatory with science instruments provided by European-led Principal Investigator consortia and with important participation from NASA. PACS: The Photodetector Array Camera and Spectrometer is one of Herschel's instruments.

Qualitatively, Centaurs are a transitional population between TNOs and Jupiter-family comets. The exact definition of a Centaur is not generally agreed upon in the literature. Gladman et al. (2008) has the most restrictive definition, which excludes Okyrhoe and Echeclus, which are both considered to be Centaurs by many. According to the Gladman classification, perihelion distance, q , and the semimajor axis, a , satisfy $a_J < a < a_N$ and $q > 7.35$ AU (a_J and a_N are the semi-major axis of Jupiter and Neptune, respectively). Moreover, the Tisserand parameter needs to be $T_j > 3.05$ for these objects. The two mentioned objects are labeled Jupiter-coupled objects in Gladman et al. (2008). The most popular definition used in the literature, which we adopt here, is that $a_J < a < a_N$ and $a_J < q < a_N$ (Jewitt 2009). In addition, the object must not be in a mean-motion resonance with any planet.

Dynamical models suggest that close encounters with planets limit the median orbital lifetime of Centaurs to approximately 10 Myr (Tiscareno & Malhotra 2003) and that the lifetime is proportional to the perihelion distance. Most Centaurs ($\sim 2/3$) will be ejected to the outskirts of the solar system, while the remainder are perturbed into the inner solar system as short-period comets, broken apart, collide with a planet, or become a temporary satellite of a planet. Some objects that transit from a Centaur to a short-period comet and back, or that scatter back to the Kuiper belt, which is believed to be the main source-region. Horner et al. (2004) found that a Centaur becomes a new Earth-crossing object every 880 years. Some authors estimated that there are about 44300 Centaurs larger than 1 km in diameter and the estimated influx from the Kuiper belt is $1/125$ yr⁻¹ (Horner et al. 2004). Horner & Wyn Evans (2006) have shown that Centaurs can be captured as trojans of Jupiter and other giant planets, that is, they are in a 1:1 mean-motion resonance with the planet, and that Trojans can also escape and become Centaurs. On the other hand, Di Sisto & Brunini (2007) estimated that SDOs are probably the main source for Centaurs and provided a far higher estimate, 2.8×10^8 , for the current population of Centaurs with $R > 1$ km. Levison & Duncan (1997) suggested that trans-Neptunian objects in unstable low-eccentricity orbits are a secondary source of Centaurs, with a corresponding population of around 1.2×10^7 .

The surface properties of Centaurs and TNOs are distinct, probably because of the different influence of surface and dynamical evolution on the two groups of objects. Processes that alter the surfaces include collisions (especially for bodies ≤ 100 km), cometary activity, and space weather. Many Centaurs seem to have heterogeneous compositions. This can be explained by fresh areas after impacts or sporadic activity (Barucci et al. 2011). Due to their rapidly evolving orbits, some Centaurs may previously have been closer to the Sun and therefore were more active, even though they are currently inactive. Polarization properties, based on a small sample of observed Centaurs, indicate that there are distinct differences in the topmost surface layers of Centaurs compared with TNOs (Belskaya et al. 2010).

Among the minor planet populations, Centaurs are unique in that their B-R colors are divided into gray and red populations instead of exhibiting a continuous range of colors (Peixinho et al. 2003). This bimodal distribution does not appear in the SDOs, the possible progenitors of the Centaurs, or in the Jupiter family comets (Jewitt 2002). Lamy & Toth (2009) found no evidence for bimodality either in their Hubble Space Telescope study of the colors of 51 comets. Peixinho et al. (2003) indicated that only the Centaurs display bimodal colors. On the other hand, TNOs exhibit a broad continuous color distribution, from neutral/gray to very red, with no statistical evidence of a color gap between

the extrema (Tegler et al. 2008, for a review). On the other hand, in a recent work it was proved that small objects, including both TNOs and Centaurs, display a bimodal structure of B-R colors at a 0.1% significance level (i.e. objects with absolute magnitude $H_R(\alpha) \geq 6.8$, or $D \leq 165$ km (for an assumed albedo $p_R = 9\%$), with the “gap” centered on B-R = 1.60 (Peixinho et al. 2012). Fraser & Brown (2012) found that all objects with $q < 35$ AU (a group that includes all Centaurs) have bimodal colors.

There is no agreed-upon explanation for the observed bimodality of the Centaur colors. Possible explanations include formation in the presence of a primordial, temperature-induced, composition gradient, or the influence of comet-like activity (or lack of it). Some Centaurs are known to exhibit activity, and Melita & Licandro (2012) explored possible connections to colors. They found that Centaurs that spend more time closer to the Sun are more neutral/gray than the others. They suggested that the neutral/gray colors may result from the formation of a lag deposit of silicate dust because more volatile ices sublimate during periods of activity.

When only optical photometry data are available, the sizes of distant, unresolved small bodies can be estimated by assuming a geometric albedo. When thermal data are also available, the size and albedo can be determined simultaneously by a radiometric technique (i.e. thermal modeling). There are only a handful of distant targets, Eris, Makemake, and Quaoar, for instance, for which a direct diameter estimate via stellar occultation is available (Sicardy et al. 2011; Ortiz et al. 2012; Braga-Ribas et al. 2013). There is also an occultation diameter for Chariklo (as yet unpublished).

For objects with occultation diameters and thermal observations, the two can be combined to provide tight constraints on the temperature distribution on the surface. The temperature distribution is controlled by factors such as surface roughness, thermal inertia, and spin vector, so there is the potential to learn significantly more for these objects than for those with only thermal or occultation constraints on their diameters.

Several years ago, Stansberry et al. (2008) reported (using the Spitzer Space Telescope) the results on 15 Centaurs with a geometric albedo in the range 2.5% to 18% and an average of $7 \pm 3\%$. The measured diameters were between 30 to 260 km (Stansberry et al. 2008). Centaurs may have lower albedos than TNOs on average. Furthermore, based on that sample, Centaurs show a stronger red color - geometric albedo correlation than TNOs on average, which has not been explained. More recently, Bauer et al. (2013) published a set of 52 Centaurs and SDOs observed with WISE. They found a mean albedo of $8 \pm 4\%$ for the entire dataset.

Only very few of the brightest Centaurs have been observed using ground-based mm/submm telescopes. The Herschel open time key program “TNOs are Cool!” observed a sample of 18 Centaurs. However, that sample significantly overlaps both the Spitzer sample and the WISE sample (with 17 of the WISE objects overlapping our Herschel sample). Here we focus primarily on understanding the combined Herschel plus Spitzer sample of 28 Centaurs, plus an additional 8 SDOs.

In the next section, the observations made with the Herschel Space Observatory (PACS instrument) are presented, together with a description of the data reduction. Section 3 describes the thermal modeling applied to the data. In section 4, the results on the observed sample are presented. In section 5 we describe an extended sample found in literature. Sections 6 and 7 present a statistical analysis and the correlations found in the sample, respectively. We discuss our results in Section 8. Finally, section 9 presents the summary and conclusions.

2. Observations and data reduction

Our sample of 18 Centaurs was observed as part of the Herschel key program “TNOs are Cool!” (Müller et al. 2009, 2010). The data were collected mainly from March, 2010 to June, 2011. Table 1 presents the complete list of targets as well as pertinent information on their orbital parameters, rotational period, and light-curve amplitude, spectral slope, and whether any ices are known to be present on their surfaces. Data were taken using the Photodetector Array Camera and Spectrometer (PACS, Poglitsch et al. (2010)) in the wavelength range 60 - 210 μm . PACS is an imaging photometer with a rectangular field of view of 1.75' x 3.5'. The short-wavelength array has a filter wheel to select between two bands: 60-85 μm or 85-125 μm . The long-wavelength band is 125-210 μm , and images are collected in that channel simultaneously with either short-wavelength band. In the Herschel-PACS photometric system these bands have been assigned the reference wavelengths 70, 100, and 160 μm and are called blue, green, and red, respectively. For more details on the acquisition, data reduction, and flux extraction of the data see Santos-Sanz et al. (2012). Here we present results for 16 of the 18 Centaurs, because Chiron and Chariklo were previously presented in Fornasier et al. (2013). Finally, the Centaurs 2006 SX₃₆₈ and (42355) Typhon were observed in the science demonstration phase (two bands only) of the same key project and were published in Müller et al. (2010). 2006 SX₃₆₈ was re-observed in the routine science phase in all three bands, and the results are presented here. In Table 2 we present the identification number of the observation, followed by the duration and mid-time of the exposure. We also present the heliocentric distance, geocentric distance, and phase angle of the observation.

Of the 18 Centaurs observed with the Herschel Space Observatory, 16 were also observed by the Spitzer Space Telescope (Werner et al. 2004; Gehrz et al. 2007) using the Multiband Imaging Photometer (MIPS, Rieke et al. (2004)). Here we used Spitzer observations at 24 and/or 70 μm to complement the Herschel observations. When the 24 μm band data are combined with the Herschel-PACS data, they provide strong constraints on the color temperature of the target spectrum. When the 70 μm band data are available, they are mostly similar to the Herschel data. The Spitzer-MIPS results for most of these Centaurs were originally published by Stansberry et al. (2008), but we also present previously unpublished flux densities for four additional Centaurs observed under Spitzer program ID 50348 (PI: D. Trilling). Only two objects from the Herschel-PACS sample were not observed by Spitzer-MIPS, 2008 FC₇₆ and 2002 KY₁₄.

All of the MIPS flux densities presented here result from a consistent reprocessing of all existing Spitzer-MIPS data for TNOs and Centaurs (Mueller et al. 2012). The reprocessing uses the same reduction techniques described in Stansberry et al. (2008), but makes use of updated ephemeris information for the targets, a key element of the data processing, particularly for the fainter targets. The flux densities given here (see Table 3) supersede the values given in Stansberry et al. (2008). For targets observed more than once with Spitzer, fluxes are given from each visit, and the relevant observation identifier (AORKEY) is given in the table notes.

The Herschel-PACS data reduction from level 0 (raw data) to level 2 (images) was made using the Herschel Interactive Processing Environment (HIPE¹) with modified scan-map

¹ Data presented in this paper were analyzed using HIPE, a joint development by the Herschel Science Ground Segment Consortium, consisting of ESA, the NASA Herschel Science

pipeline scripts optimized for the “TNOs are Cool!” key program. After identifying the target we measured the flux densities at the photo-center position using DAOPHOT routines (Stetson 1987) for aperture photometry. A detailed description of how aperture photometry is implemented in our program is given in Santos-Sanz et al. (2012), Vilenius et al. (2012), Mommert et al. (2012), and Fornasier et al. (2013). The absolute photometric accuracy of our pipeline, based on the photometry of relatively faint standard stars, is explained in Kiss et al. (2013). The color-corrected flux densities are given in Table 3. The uncertainties given there include the photometric 1σ and absolute calibration 1σ uncertainties.

3. Thermal modeling

The main objective of this work is to obtain diameters, albedos, and surface thermal properties of the targets. Our targets are too small to resolve by direct-imaging, but by combining visible, reflected-light measurements and thermal measurements, it is possible to solve for the geometric albedo and size, and in some cases also to constrain the surface temperature distribution. This *radiometric technique* relies on a model that describes how thermal radiation is emitted from the surface of the targets, and is briefly described below.

The flux density of reflected solar light depends on the product of the target’s size and albedo. Using the definition of absolute magnitude H , this is expressed by

$$H = m_{\text{Sun}} + 5 \log \left(\sqrt{\pi} a \right) - \frac{5}{2} \log \left(p S_{\text{proj}} \right), \quad (1)$$

where m_{Sun} is the visual magnitude of the Sun, a is the distance of 1 AU in km, p is the geometric albedo, and S_{proj} is the projected area of the target in km^2 . H , m_{Sun} and p are expressed in the same pass-band, usually V or R band. For the majority of Centaurs, H_V magnitudes were computed using literature values. For some targets we calculated a new H_V based on apparent magnitudes, corrected for the observing geometry, and performed a linear fit to determine the phase correction. A few targets do not have photometric-quality data available; for these we used the Minor Planet Center data, usually in R-band, together with the average V-R color of Centaurs from the MBOSS-2 data base.

There are three basic types of models to predict the emission of an airless and coma-less body with a given size and albedo assuming an energy balance between insolation and re-emitted thermal radiation: the standard thermal model (STM) (Lebofsky et al. 1986), the fast-rotator or isothermal-latitude thermal model (ILM) (Veeder et al. 1989), and the thermo-physical model (Spencer et al. 1989; Lagerros 1996, e.g.). The STM assumes a spherical body where temperatures on the surface depend on the angular distance ω from the subsolar point as in a Lambertian emission model:

$$T(\omega) = \cos^{\frac{1}{4}}(\omega) \left[\frac{(1-A) S_{\text{sun}}}{\epsilon_b \eta \sigma r^2} \right]^{\frac{1}{4}}, \quad (2)$$

where A is the Bond albedo, S_{sun} the bolometric solar constant, ϵ_b the bolometric emissivity, σ the Stefan-Boltzmann constant, and r the heliocentric distance. Since the optical constraint (Eq. 1) is often used with V-band data and the temperatures

Center, and the HIFI, PACS and SPIRE consortia members, see <http://herschel.esac.esa.int/DpHiPeContributors.shtml>

(Eq. 2) depend on $1-A = 1-pq$, where q is the phase integral, we assumed that $A \approx A_V$ and used $q = 0.336 p_V + 0.479$ derived by Brucker et al. (2009) for a sample of TNOs. The beaming parameter, η , is an empirical factor that adjusts the subsolar-point (i.e. maximum) temperature. It approximately accounts for the combined effects of roughness, thermal inertia, and rotational period. On rough surfaces heat is radiated preferentially in the sunward direction, which means a beaming factor $\eta < 1$. Values of $\eta > 1$ mimic the effects of high thermal inertia (or fast rotation).

While the STM discussed above makes the simplifying assumption that the object has zero thermal inertia, the ILM is the opposite extreme, assuming infinite thermal inertia. In consequence, the ILM temperature distribution is isothermal at any given latitude, and represents the coldest end-member model for the temperature distribution.

As in our previous ‘‘TNOs are Cool’’ key program publications (Santos-Sanz et al. 2012; Vilenius et al. 2012; Mommert et al. 2012), we used models derived from the STM: either the Near-Earth Asteroid Thermal Model (NEATM) (Harris 1998) or the hybrid-STM (Stansberry et al. 2008). Except for the fact that the hybrid-STM assumes zero phase angle, it is identical to NEATM. Because all of our targets are observed at phase angles smaller than 10 deg, the differences between the two models is expected to be small. However, thermal phase curves of Centaurs and TNOs are poorly understood, so it is difficult to quantify exactly how large the differences might be. In the canonical STM formulation $\eta = 0.76$ (Lebofsky et al. 1986), but in the NEATM model η is adjusted, that is, it is allowed to ‘‘float’’, to best fit the observed emission from each target.

For each target we fit the NEATM to three fluxes (for the Herschel-only targets), or to four or five fluxes (for the Herschel plus Spitzer targets, depending on whether only the 24 or the 24 and 70 μm data were available). If these floating- η fits to the data resulted in un-physical values for η (< 0.6 or > 2.6), we instead fit the data using $\eta = 1.2 \pm 0.35$, based on the average value for TNOs and Centaurs found by Stansberry et al. (2008). Based on beaming parameters measured for 85 TNOs and Centaurs, Lellouch et al. (2013) found median and equal-weight mean values of $\eta = 1.09$ and 1.175, respectively. Their Figure 1 shows that nearly all objects at heliocentric distances smaller than 30 AU have beaming parameters in the range 0.8-1.7, consistent with the range of values we have assumed above. Lellouch et al. (2013) interpreted the η values in terms of a very low thermal inertia of the TNO/Centaur population.

A simplifying assumption we made (which has been made in previous publications from our team and from other groups) is that the nonspherical shape of the objects can be neglected when applying the radiometric method to derive sizes and albedos. Most TNOs are large enough to probably be almost spherical (the smaller ones, which might have irregular shapes, are too faint to have been discovered). Our Centaur sample, however, includes many objects small enough to be nonspherical, and several are known to have significant rotational light-curves, as summarized in Table 1.

To precisely account for the effects of nonspherical shapes on our results, our modeling would have to account for the exact light-curve phase of each observation, allowing for the area of the target to be a function of time. A complication with this approach arises because the measured rotational periods of some targets are too imprecise to allow for accurate phasing with our data. Furthermore, our thermal observations typically are rather long, so the data from even a single-band observation sample a range of rotational phases. Moreover, our multiband data (even if only the Herschel data are considered) are acquired at multi-

ple epochs, with four separate epochs applying at both 70 μm and 100 μm , and eight epochs at 160 μm . The signal-to-noise (S/N) ratio achieved in any single-epoch observation is typically low because our observations were designed to achieve a S/N of about 10 when all epochs are co-added. Thus, the particulars of our Herschel data sets for Centaurs complicate any attempt to model our rotating targets in a fully self-consistent way as regards their cross-sectional area as a function of time. Mitigating these complications somewhat is the fact that modeling of thermal emission from non-spherical objects shows that thermal light-curves are generally more subdued than they are in the visible (Santos-Sanz et al. 2012).

To avoid these complications but allow for the effects of non-spherical shapes on our results, we systematically applied larger uncertainties to our H magnitudes, as described in Vilenius et al. (2012). For the objects with measured light-curves, we added 88% of the half-amplitude quadratically to the formal uncertainty on the measured H magnitude. For objects with unknown light-curve amplitude, we assumed a light-curve half-amplitude of 0.2 mag. For objects such as Pholus and Asbolus, with strong light-curves, this results in an effective uncertainty of 0.3 – 0.4 mag. By making this adjustment to the H magnitudes we used in our modeling, the error bars we derived on the albedo, diameter, and beaming parameter are expected to encompass the actual values for our targets.

4. Results using Herschel-PACS

All the measured fluxes using Herschel-PACS and the new (updated or previously unpublished) fluxes from Spitzer are included in Table 3 together with the absolute magnitude, diameter, albedo and η from the thermal modeling. The error estimates of the geometric albedo, the diameter and the beaming parameter were determined by a Monte Carlo method, as described in more detail on Müller et al. (2010), Santos-Sanz et al. (2012), and Mommert et al. (2012).

In this section we describe each target and also include information on the spectral signatures that give clues on the ices present on the surface of the targets. The information on the overall spectral shape in the visible and near-infrared is presented using the Barucci taxonomy (Barucci et al. 2005) and updates on that work presented in Fulchignoni et al. (2008) and Perna et al. (2010).

Objects with a neutral/gray color with respect to the Sun are classified as the BB (blue or gray) group, and those with a high red color are classified as RR (red). The BR group consists of objects with an intermediate blue-red color, while the IR group includes moderately red objects. In our analysis we used the spectral slope in the visible that has been widely interpreted as an indication of surface composition. Steep red slopes have typically been associated with complex organics (tholins) on the surface (Cruikshank et al. 2005). Neutral/gray slopes, on the other hand, are related to highly processed surfaces covered by dark carbonaceous materials (Andronico et al. 1987) or high-albedo water-ice-rich surfaces (Pinilla-Alonso et al. 2008). All these variables are presented in the last two columns of Table 1.

Centaurs are mainly distributed in the BR and RR classes, with a similar H₂O-ice-content distribution. There are no Centaurs with an abundant surface-ice content, that is, higher than 20% (Barucci et al. 2011). The majority of Centaurs observed multiple times have a heterogeneous composition. This seems to be the main characteristic of the Centaur population: the variation that affects the new areas that surfaced or were altered by impacts while the Centaurs were still in the transneptu-

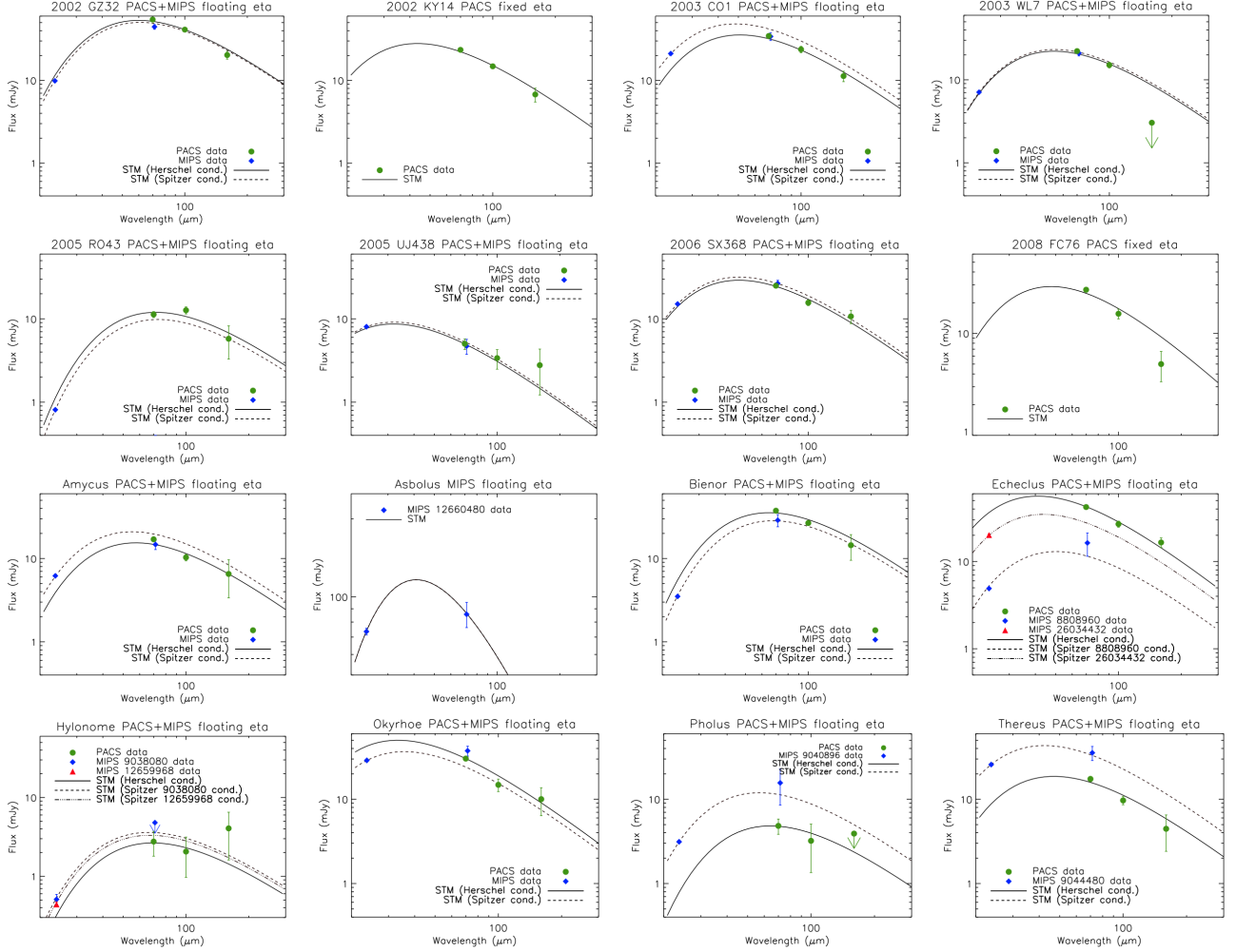


Fig. 1. Thermal modeling of all the Herschel targets. For PACS+MIPS plots the filled line is the best-fit (hybrid-STM) for the geometrical Herschel targets, at the heliocentric distance $r(h)$ and geocentric distance Δ conditions. The dashed line is the best-fit using the same model but for the Spitzer geometrical conditions. As discussed in the text, the preferred solution for Pholus is the one with AORKEY 12661760.

nian region. This variation may also have been caused by temporal or sporadic activity.

4.1. Results on individual targets

In this subsection we present the results and all the information we consider important for modeling and interpreting the results for each individual object. The rotational period, which is useful in thermo-physical models, and the light-curve amplitude, which one needs to know to determine how spherical the object is or how inhomogeneous the surface, are also presented in Table 1. Information on the spectral slope is also presented and included in the same table. Here we give information on the spectral signatures, which give clues on the ices present on the surface of the targets. The spectral information (visible spectral slopes) is used below to determine the correlation between size/albedo and surface composition. If cometary activity was reported on the object it is indicated here.

(95626) 2002 GZ₃₂: has a BR spectral type with a tentative indication of water ice in the surface (Barucci et al. 2008). Our results indicate that it is the largest object of the sample with

$D = 237 \pm 8$ km, a low albedo of 3.7 ± 0.4 %, and $\eta = 0.97^{+0.05}_{-0.07}$. We used Spitzer-MIPS data to fit a thermal model with five points. No cometary activity was reported in the literature. The light-curve indicates a rotational period of 5.80 ± 0.03 hours with a low amplitude of 0.08 ± 0.02 magnitudes (Dotto et al. 2008). This object is spectrally gray with a moderately small spectral gradient of $8\%/10^3 \text{ \AA}$. This object has an indication of a weak absorption band centered around 4300 \AA (wide 200 \AA and a depth of about 3% with respect to the continuum). If real, this feature would be similar to the absorption at 4300 \AA found on some primitive main-belt asteroids and attributed to a ferric iron Fe^{3+} spin forbidden absorption in minerals derived from the aqueous alteration process such as iron sulfate jarosite (Fornasier et al. 2004).

(250112) 2002 KY₁₄: also known as 2007 UL₁₂₆, has RR spectral type with an indication of water ice in the surface (Barucci et al. 2011). Thirouin et al. (2010) reported a rotational one-peak period of $3.56/4.2 \pm 0.05$ hours with an amplitude of 0.13 ± 0.01 magnitudes. In our results we tried to model it with a floating η but the fit was not acceptable, so we applied a fixed

η model. From the fixed η of 1.20 ± 0.35 our preferred solution is a diameter of 47_{-4}^{+3} km and an albedo of $5.7_{-0.7}^{+1.1}\%$. Only the Herschel-PACS fluxes were fitted because there are no Spitzer observations of this object.

(281371) 2008 FC₇₆: Fornasier et al. (2009) reported a spectral slope of $36.0 \pm 0.7\%/10^3 \text{ \AA}$. The spectral type is RR with no detection of water ice or any other ices in the surface (Barucci et al. 2011). Its rotational period is not known yet. No activity was observed in this object. Our results indicate that the object has a 68_{-7}^{+6} km diameter with an albedo of $6.7_{-1.1}^{+1.7}\%$. This object was modeled with only the three Herschel-PACS fluxes, using a fixed η model.

(136204) 2003WL₇: has a BB spectral type (Barucci et al. 2011). Light-curve information is provided by Thirouin et al. (2010), who reported a single-peak rotational period of 8.24 ± 0.05 hours with an amplitude of 0.05 ± 0.01 magnitude. The fitted model to the five points (Herschel + Spitzer) gives a diameter of 105_{-7}^{+6} km, an albedo of $5.3 \pm 1\%$, and an $\eta = 1.02_{-0.05}^{+0.07}$. The flux at $160 \mu\text{m}$ is an upper limit and is below the fitted model.

2005 RO₄₃: there are no works in the literature that describe the physical properties of this object. In our case, the fitted model to the five points (Herschel + Spitzer) gives a diameter of 194 ± 10 km, an albedo of $5.6_{-2.1}^{+3.6}\%$, and an $\eta = 1.12_{-0.08}^{+0.05}$. There is an excess in flux at $100 \mu\text{m}$ (see Fig. 1).

(145486) 2005 UJ₄₃₈: this is the smallest object of our sample. Our results using a free $\eta = 0.34_{-0.08}^{+0.09}$ indicate that the object has a 16_{-2}^{+1} km diameter with an albedo of $25.6_{-7.6}^{+9.7}\%$. This surprising low η could be indicative of activity. In some sense the high albedo is a direct effect of the low η . The object was at the detection limit, around 5-6 mJy at PACS wavelengths. The results on this object presented by Bauer et al. (2013) also included a high albedo, in this case obtained through a fixed η model. Lellouch et al. (2013) also mentioned that this object has an extremely low η value. This might result from coma activity, because emission of small and hot particles would enhance the short-wavelength flux, leading to a low apparent η .

(248835) 2006 SX₃₆₈: in a previous work of the TNOs are Cool! program (Müller et al. 2010) we reported a fixed η -approach modeling that yielded a diameter of 79 ± 9 km and $p_v = 5 \pm 1\%$. This object is BR in the taxonomy. It is on a very eccentric orbit, near the 5:4 mean motion resonance with Uranus. In Müller et al. (2010) the Herschel-PACS $70 \mu\text{m}$ detection was compatible with diameters in the range of 70-80 km and an albedo of 5-6%, consistent with our results. The upper $160 \mu\text{m}$ flux limit in that work constrains the diameter range to values below 105 km and an albedo higher than 3%, both in agreement with the measured $70 \mu\text{m}$ -flux. No light-curve is published for this objects. Jewitt (2009) reported this object as active. Fulchignoni et al. (2008) classified it as BR type. Recently, Perna et al. (2013) searched for signs of activity in this object, with negative results, which sets limits on the dust production rate. Our results, including the Spitzer values, gives a diameter of 76 ± 2 km, with an albedo of $5.2_{-0.6}^{+0.7}\%$, and a final floating $\eta = 0.87_{-0.06}^{+0.04}$.

(120061) 2003 CO₁: the spectral type of this object is BR (Perna et al. 2010). Analysis of the light-curve of this object

in two different works resulted in two different estimate for the rotational period: 10.00 ± 0.01 hours with an amplitude of 0.10 ± 0.05 (Ortiz et al. 2006), and a single-peak rotational period of 4.51 ± 0.05 hours with an amplitude of 0.07 ± 0.01 magnitudes reported by Thirouin et al. (2010). There is a tentative detection of water ice in the surface (Barucci et al. 2011). This object has Spitzer observations that combined with those of Herschel-PACS give five points to be fitted with the thermal model. The final results give a diameter of 94 ± 5 km, an albedo of $4.9_{-0.6}^{+0.5}\%$, and $\eta = 1.23_{-0.11}^{+0.12}$.

Amycus: the reported spectral type is RR with a tentative detection of water ice in the surface (Barucci et al. 2011). Our results indicate that the object has a 104_{-8}^{+8} km diameter with an albedo of $8.3_{-1.5}^{+1.6}\%$ and $\eta = 1.00_{-0.13}^{+0.12}$. The thermal model fit presents a flux excess at $24 \mu\text{m}$, which may be related with two different albedo terrains, as was suggested in Lim et al. (2010) for Makemake. The light-curve gives a rotational period of 9.76 hours with an amplitude of 0.16 magnitudes (Thirouin et al. 2010). The compositional spectral model indicates amorphous carbon, Triton tholin and water ice in the surface (Doressoundiram et al. 2005), which is compatible with the RR type.

Bienor: is a BR spectral type Centaur with a positive detection of water ice in the surface (Barucci et al. 2011). Our results indicate that this object has a 198_{-7}^{+6} km diameter with an albedo of $4.3_{-1.2}^{+1.6}\%$ and a $\eta = 1.58_{-0.07}^{+0.07}$. The reported rotational period is 9.14 hours with an amplitude of 0.75 magnitudes, or 9.174 ± 0.001 hours with an amplitude of 0.34 ± 0.08 magnitudes (Ortiz et al. 2002, 2003).

Echeclus: There are two different Spitzer-MIPS observations, but the fitted model gives compatible results. The preferred result is the one using the two Spitzer observations combined with the Herschel observation. Our results indicate that the object has a 64.6 ± 1.6 km diameter with an albedo of $5.20_{-0.71}^{+0.70}\%$ using an $\eta = 0.861_{-0.036}^{+0.037}$. Figure 1 shows the fit with MIPS AORKEY 26034432 and 8808960 and the Herschel observation. No light-curve information is present in the literature.

Neither is there a spectral signature indicating ices on the surface (Guilbert et al. 2009). This object presented a peculiar cometary activity. The source of cometary activity appears to be distinct from Echeclus itself. The brightness distribution of this source does not follow that of a cometary coma created by a point-like source (cometary nucleus). It was reported to look like a diffuse source (Rousselot 2008). Bauer et al. (2008) suggested -based on Spitzer imaging- that this Centaur had sustained activity. Echeclus has recently turned on again (IAU Circular 9213), which makes it very likely that its cometary activity is related to volatile sublimation or water-ice crystallization and not triggered by an unknown external phenomenon.

Hylonome: in this case, there are also two different observations with Spitzer. The adopted value was the combination of these two observations with that of Herschel one. Our results indicate that the object has a 74 ± 16 km diameter with an albedo of $5.1_{-1.7}^{+3.0}\%$ and an $\eta = 1.29_{-0.31}^{+0.31}$. No light-curve information is present in the literature. Figure 1 only shows the fit with one of the MIPS AORKEY 9038080. The fit with the other MIPS AORKEY is very similar.

Okryhoe: our results indicate that the object has a 35 ± 3 km diameter with an albedo of $5.6^{+1.2}_{-1.0}\%$ and $\eta = 0.71^{+0.12}_{-0.13}$. No light-curve information is available in the literature. Barucci et al. (2011) reported a tentative detection of water ice in the surface and classified this object as a BR in the taxonomy.

Pholus: our preferred results is the one using Spitzer AORKEY 9040896 and Herschel observations because the other Spitzer AORKEY has no $70 \mu\text{m}$ detection. The object has a 99^{+15}_{-14} km diameter with an albedo of $15.5^{+7.6}_{-4.9}\%$ and an $\eta = 0.77^{+0.16}_{-0.16}$. This object has a reported rotational period of 9.98 ± 0.01 hours with different amplitudes ranging from 0.15 to 0.60 magnitudes (Buie & Bus 1992; Hoffmann et al. 1992; Perna et al. 2010). The reported spectral class is RR (Perna et al. 2010). The spectral information shows a clear indication of water ice in the surface (Barucci et al. 2011; Guilbert-Lepoutre 2012). There is also an indication of methanol (CH_3OH) in the spectra of this object (Barucci et al. 2011).

Thereus: our results indicate that the object has a 62^{+3}_{-3} km diameter with an albedo of $8.3^{+1.6}_{-1.3}\%$ and an $\eta = 0.87^{+0.08}_{-0.08}$. The reported rotational period is 8.33 ± 0.01 hours from different sources (Ortiz et al. 2002, 2003; Rabinowitz et al. 2007; Brucker et al. 2008). The light-curve amplitude is 0.16-0.18 or its double 0.34-0.38. Its classification is in the BR taxonomy type. Licandro & Pinilla-Alonso (2005) detected spectral rotational variation and modeled the surface with amorphous carbon silicates, tholins, and different water-ice quantities.

Asbolus: the preferred solution considered only MIPS 12660480 observations. We discarded MIPS 9039360 because the Spitzer fluxes are probably affected by activity. There was a great change in heliocentric distance between both MIPS observations. We tried to fit the two MIPS fluxes separately with the Herschel-PACS fluxes without acceptable result. The selected solution was the one with the strongest signal, that is the one with the shorter heliocentric distance. The adopted solution gives an estimated diameter of 85^{+8}_{-9} km, an albedo of $5.6^{+1.9}_{-1.5}\%$, and an $\eta = 0.97^{+0.14}_{-0.18}$.

Finally, there is a list of Centaurs observed with Spitzer-MIPS, some of them published in Stansberry et al. (2008). Here, we used updated values for Nessus, Elatus, Cyllarus, Crantor, and 2001 BL₄₁. Moreover, we included in the analysis four objects observed with Spitzer-MIPS that have not yet been published: (119315) 2001 SQ₇₃, 2002 VR₁₃₀, 2004 QQ₂₆, and 2000 GM₁₃₇. Model results for the two objects observed only with Spitzer-MIPS (updated and unpublished) are shown in Fig 2.

The final sample of Centaurs we analyzed (Fig. 1 and Fig. 2) consists of 14 objects observed with Herschel-PACS and Spitzer-MIPS, 2 Centaurs observed only with Herschel-PACS (2008 FC₇₆ and 2002 KY₁₄) and 9 objects observed only with Spitzer-MIPS (including four that were previously unpublished).

5. Extended Centaur sample observed with Herschel

Here we describe the radiometric diameters and albedos for Centaurs derived from the literature. We combine these results with those presented above for the statistical and correlation analysis presented in the next section.

Chiron and Chariklo were observed with the Herschel PACS and SPIRE instruments at 70, 100, 160, 250, 350, and 500 μm .

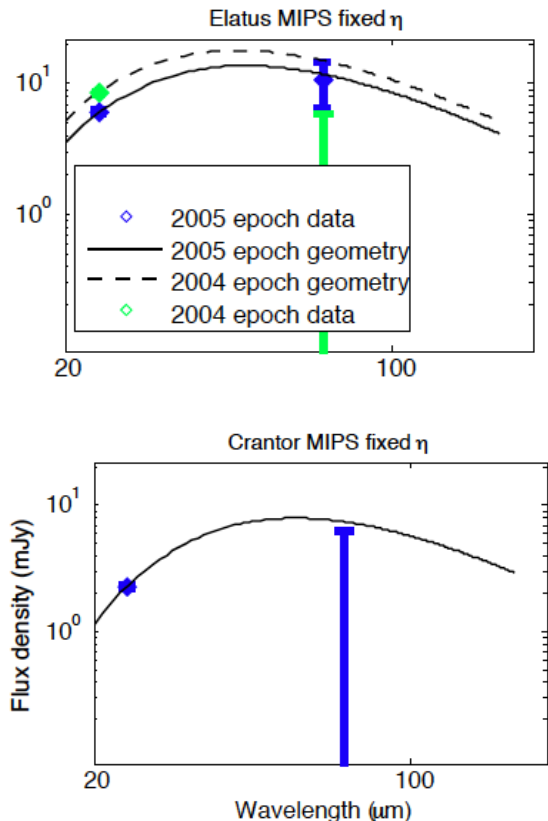


Fig. 2. Thermal modeling of two of the new or re-modeled Spitzer-only observed Centaurs. Only these two targets had two-band data. In the particular case of Crantor the upper limit at $60 \mu\text{m}$ was treated as a data point with zero flux and 1σ error-bar, equaling the upper limit value (0 ± 6.31 mJy). The model for Crantor also considers a fixed η . The other Spitzer-only objects are modeled with only one point at $24 \mu\text{m}$ and with fixed η .

The results were presented in Fornasier et al. (2013) and are summarized below along with other results.

Chiron: this is the first discovered Centaur and the first with detected activity. Some changes in the intrinsic brightness were detected by Hewitt and Bowell in 1978, described in Bus et al. (1989), and the sudden brightening of Chiron between 1988 and 1989 (Tholen et al. 1988; Bus et al. 1988; Hartmann et al. 1990) confirmed the cometary nature of this object. The coma around Chiron was first detected by Meech & Belton (1989) when it was at a heliocentric distance of 11.8 AU. Both long-term (months to years) and short-term (hours to days) variations in Chiron's absolute magnitude have been identified and are attributed to ongoing, episodic cometary activity. These variations were analyzed in detail by Duffard et al. (2002) and updated more recently by Belskaya et al. (2010). The variation of H_V over nearly 40 years shows several peaks of activity, with the absolute magnitude changing by as much as two magnitudes as a result of cometary activity.

In addition to the spectral signatures attributed to water ice on its surface (Foster et al. 1999), Chiron is one of the largest known Centaurs. However, estimates of its size vary consider-

ably (perhaps because the contribution of the dusty coma has not been accounted for). Using various techniques the diameter of Chiron has been estimated to be 180 km (Lebofsky et al. 1984), 372 km (Sykes & Walker 1991), and 182-189 km (Campins et al. 1994; Marcialis et al. 1994). Fernández et al. (2002) found a diameter of 148 ± 8 km with an albedo of 0.17 ± 0.02 and Groussin et al. (2004) found a radius of 142 ± 10 km.

More recently, Fornasier et al. (2013) analyzed Herschel PACS and SPIRE data for Chiron (assuming $H_V = 5.92 \pm 0.20$). Based on their thermal modeling, Chiron's diameter is 218 ± 20 km, and its geometric albedo is $16 \pm 3\%$. These authors considered the effect of Chiron's coma in some detail and estimated that at the time of the Herschel observations the coma contributed no more than 4% to the observed fluxes. There was no evidence of a resolved coma in these data, and the authors were able to set an upper limit on the dust production rate (based primarily on the PACS $70 \mu\text{m}$ data).

Chariklo: The Spitzer telescope observed Chariklo at 24 and $70 \mu\text{m}$ using MIPS. Chariklo was also observed with the Widefield Infrared Survey Explorer (WISE) at 11.6 and $22.1 \mu\text{m}$ (Wright et al. 2010). Fornasier et al. (2013) combined Herschel observations with those of Spitzer and WISE.

Assuming an $H_V = 7.40 \pm 0.25$ magnitude corresponding to the absolute magnitude estimate that is closest to the observations (March-June 2008, from Belskaya et al. 2010), the diameter derived from the NEATM model of the revised Spitzer-MIPS and Herschel PACS and SPIRE data is $D = 236.8 \pm 6.8$ km and a geometric albedo of $3.7 \pm 1\%$. Including WISE data, the preferred solution using the TPM method and all the observed wavelengths is $D = 248 \pm 18$ km and an albedo of $3.5 \pm 1\%$.

The fact that the TPM model excludes the pole-on solution at the time of the Herschel observations reinforces the assumption made by Belskaya et al. (2010), who speculated that the 2007-2008 observations after the Chariklo passage at perihelion (corresponding to a fainter H_V magnitude) were made viewing the equator, while the 1999-2000 observations, which show a higher H_V value and short-term brightness variations, corresponded to a pole-on geometry. For the surface composition, Dotto et al. (2003) reported the spectral signature for water ice in the surface of Chariklo.

An important conclusion of Fornasier et al. (2013) is that both Chiron and Chariklo show a significant decrease of emissivity for wavelengths $\geq 100 \mu\text{m}$. The decrease in emissivity at very long wavelengths probably means that at these wavelengths the top surface layer becomes more transparent and we see the subsurface (which has lower temperatures and higher thermal inertias).

There are two other Centaurs observed previously with Herschel. As reported in Müller et al. (2010), Typhon was observed in the science demonstration phase; additional observations were presented in Santos-Sanz et al. (2012), who included it in their sample of SDO's. The object 2006 SX₃₆₈ was observed in the science demonstration phase. These data have not been previously published, therefore we analyzed them and include the results here.

Typhon: Müller et al. (2010) reported on Herschel science demonstration phase observations of the binary Centaur, Typhon, finding $D = 138 \pm 9$ km, $p_V = 8 \pm 1\%$, and $\eta = 0.96 \pm 0.08$. Their analysis was based on both Spitzer and Herschel fluxes. The object has a rotational period of 9.67 hours and a light-curve amplitude of 0.07 ± 0.01 magnitudes.

Typhon was also observed in the science routine phase in the three Herschel-PACS bands. Results were published in Santos-

Sanz et al. (2012), presenting a diameter of 185 ± 7 km, an albedo of $4.4 \pm 0.3\%$, and an η value of 1.48 ± 0.07 . As mentioned in Santos-Sanz et al. (2012), the SDP observations were performed in chop-nod mode (less sensitive than scan-map for point-sources), which gives lower 70 and $100 \mu\text{m}$ fluxes and no detection at $160 \mu\text{m}$. In this work we prefer the results of Santos-Sanz et al. (2012). Typhon is a Centaur according to the MPC and an SDO according to the Gladman definition. We include this object in the final complete (Centaurs + SDOs) sample.

By combining their Herschel diameter for Typhon with the system mass determined by Grundy et al. (2008), Santos-Sanz et al. (2012) derived a bulk density of $0.66^{+0.09}_{-0.08} \text{ g cm}^3$. This is slightly higher than the value reported by Grundy et al. (2008), who used the diameter reported by Stansberry et al. (2008), based on a single-band Spitzer detection.

6. Statistical analysis

In this and the next section we analyze our results on Centaurs and search for correlations between the albedo and the diameter and some of their physical characteristics, such as orbital parameters and visible spectral slope. When we do not specify otherwise, we refer to the whole sample of Centaurs together with the sample of SDOs.

The geometric albedos for our sample are mostly lower than 13% with two exceptions, 2005 UJ₄₃₈ with $25.6^{+9.7}_{-7.6}\%$ and Chiron with an albedo of $16 \pm 3\%$ (the only one considered active at the time of observation by Herschel). The albedo of 25% for 2005 UJ₄₃₈ and the $\eta = 0.34 \pm 0.09$ indicate that this object might be active or has been active recently. The data indicate a color temperature of ~ 161 K. This is higher than the instantaneous sub-solar temperature of a zero-albedo object at the relevant heliocentric distance, 136 K (hence the low equivalent η value that is obtained within a NEATM). Therefore this high color temperature might be due to superheated small dust grains. This requires the grains to be small; otherwise they would have the same temperature as the nucleus. The darkest object is Chariklo with an albedo of $3.5 \pm 1\%$ followed by 2002 GZ₃₂ with an albedo of $3.7 \pm 0.4\%$. The mean albedo for our sample is $6.9 \pm 4.8\%$ for the Centaur population and $6.7 \pm 4.8\%$ considering the entire Centaur and SDO sample. As can be seen in Fig. 3 (right plot), there is a concentration of objects with albedos between 2 and 6% that comprises 61% of the sample. The other 39% show more disparate values between 6 and 26%. Including SDOs in the sample yields similar results, with 65% concentrated in the 2 - 6% range (see Fig. 3).

In the Centaur sample (Herschel sample) the largest object is 2002 GZ₃₂ with a diameter of 237 ± 8 km, and the smallest is 2005 UJ₄₃₈ with a diameter of 16^{+1}_{-2} km. When we include the Spitzer sample, the smallest Centaur is 2000 GM₁₃₇ with 8 ± 1.5 km in diameter. In the whole sample, 82% of the objects are smaller than 120 km in diameter. SDOs in our sample are consistently larger than the Centaurs, only one is smaller than 120 km (2002 PN₃₄ with a diameter of 112 ± 7 km). This is a clear discovery/observational bias. In Fig. 3, left panel, we show that the distribution of sizes in the sample of Centaurs and Centaurs plus SDOs is not continuous, there is a gap from 120 to 190 km where we can find only one object, 2002 XU₉₃ an SDO with a diameter of 164 ± 9 km. 71% of the objects are smaller than 120 km.

The separation into small and large objects in the Centaur and TNO population is not new. The small objects in these populations, those with a diameter < 150 km, are thought to be frag-

ments from collisions of larger ones. This is an interesting point because their surfaces may have been remodeled by the impact. Peixinho et al. (2012) stated a limit of 165 km using a mean albedo of 9%. In our sample we have no objects between 120 km and 190 km, therefore we took 120 km as the limit to distinguish between small and large objects. The mean albedo for our small and large Centaurs is $7.0 \pm 4.0\%$ and $6.2 \pm 5.0\%$, respectively. They are not distinguishable within the errors which suggests that there is no clear dependence of the albedo and size of this objects. We study this and other correlations in the next section.

Following what is shown in Fig. 3 that most of the centaurs are small, and most of the centaurs are dark, one can ask here whether these two most common populations in the size and albedo distribution (the small Centaurs and the low-albedo objects) are related. Are the most abundant small Centaurs also the darkest? Figure 4 clearly shows that this is not true, because the albedo of the small Centaurs takes any value from 4% to 14%. That interval represents almost the entire range of albedos for the whole population (4% - 16%). Qualitatively, the albedos of the small objects are not different from the albedo of the whole sample (including the scattered objects), with the exception of 2005 UJ₄₃₈ which we commented above.

Recently, Bauer et al (2013) published a statistical analysis of 52 centaurs and SDOs observed with WISE. Our results are similar to theirs. There are 17 objects in common in both samples. Both the diameters and the albedo estimate are similar within the error bars, discarding any systematic deviation of one set of results with respect to the other. For most of the sample, our results are more precise therefore, even if our sample is smaller than theirs, our results complement the previous ones because they provide better estimate of both diameter and albedo. However, there are some particular objects where the results are clearly different above the 1σ limit. The diameter of Thereus is larger for the WISE fit (86.5 ± 1.9 km) than our result (62 ± 3 km). The albedos estimated for Chariklo, 2002 KY₁₄, and 2008 FC₇₆ are $7.5 \pm 1.5\%$, $18.5 \pm 4.6\%$ and $12.0 \pm 2.7\%$ using WISE data, these values are higher than our estimate ($3.5 \pm 1.0\%$, $5.7 \pm 1.0\%$, and $6.7 \pm 1.5\%$, respectively).

Different factors might be the origin of these difference such as the use of a different value of the absolute magnitude, or fits of the fluxes using only one or two bands instead of four for the WISE data, or two fluxes instead of three for the Herschel data. However, we investigated these effects and there is no consistent explanation for these differences. We believe that a combination of these and other factors, such as the S/N of the observations, might be the cause of the disparity. The case of Amycus is different. Both results are compatible within the errors, either the diameter or the albedo, but the error bar is much larger for WISE (by a factor of 5 for the diameter and ~ 10 for the albedo), which may indicate that there is a problem with the WISE data or the reduction for this object. Our result ($D=104 \pm 8$ km and $pv=8.3 \pm 1.5\%$) is probably more reliable for this object. These differences affect the average values slightly. Bauer found a mean albedo of $8 \pm 4\%$, we found a similar value of $6.9 \pm 4.8\%$ for the Centaurs and $6.7 \pm 4.8\%$ for the whole sample.

7. Correlations

Correlations of albedo, diameter, and beaming parameter with parameters such as inclination i , eccentricity e , semi-major axis a , perihelion distance q , aphelion distance Q , and heliocentric distance at the moment of observation, $r(h)$, (e.g. orbital parameters, visible spectral slope) have been discussed in previous stud-

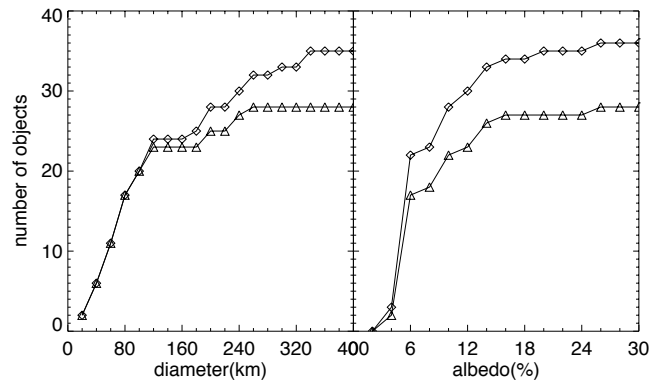


Fig. 3. Cumulative distribution for diameters and albedo for the whole sample (Centaurs + SDOs, squares) and Centaurs only (triangles). In the left panel 2007 OR₁₀ is excluded because its diameter ($D=1280$ km) is beyond the scale.

ies of TNOs. We searched for such correlations within our sample using a modified Spearman rank correlation test, taking into account symmetrical and asymmetrical error-bars (Spearman 1904; Peixinho et al. 2004; Santos-Sanz et al. 2012). Roughly speaking, a correlation is said to be strong when $|\rho| > 0.6$. However, the evidence for a correlation is given by the significance level, or equivalently by the confidence level, not by the value of the correlation coefficient. That is, if we measure a correlation of $\rho = 0.8$, but achieve a significance of only 0.2 (i.e. a 20% probability of being a random effect), the correlation is considered to be statistically insignificant. Table 4 shows correlation coefficients and the corresponding significance values and confidence levels for all of the parameter combinations we have examined. The strongest correlations are highlighted in boldface.

To increase the sample, we also considered diameters and albedos of the eight SDOs from Santos-Sanz et al. (2012). We analyzed the results as the whole sample (Centaurs+SDOs) and separately (Centaurs only). We also defined a third group corresponding to objects smaller than 120 km, based on the findings of Peixinho et al. (2012) and Fraser & Brown (2012). Because 2007 OR₁₀ lacks a published visible spectrum, but has an NIR spectrum similar to that of Quaoar (Brown et al. 2011), we assumed that their visible spectral slopes are the same.

The only strong correlation found for the Centaurs is between diameter and heliocentric distance (figure 5, bottom). This correlation persists and is even stronger when we added the SDOs to the sample. When we considered only the smaller Centaurs, this correlation is weaker but still present. This is probably an observational bias that we discuss below.

When we consider the full sample, the correlation between diameter and semi-major axis, perihelion distance, and inclination are strong. However, the correlation between diameter and eccentricity is weak for the full sample, and that between diameter and eccentricity becomes weaker for the Centaur sample alone.

For the smaller Centaurs there are only weak correlations, such as for albedo versus spectral slope, diameter versus semi-major axis, and diameter versus heliocentric, perihelion, and aphelion distances. We note that for the Centaurs, whit significant orbital eccentricities, all of these distances are correlated, so their correlations with the physical parameters should be, and are, similar.

We do not find evidence for a correlation between albedo and diameter in our sample (see Fig. 4). We cannot say the same for

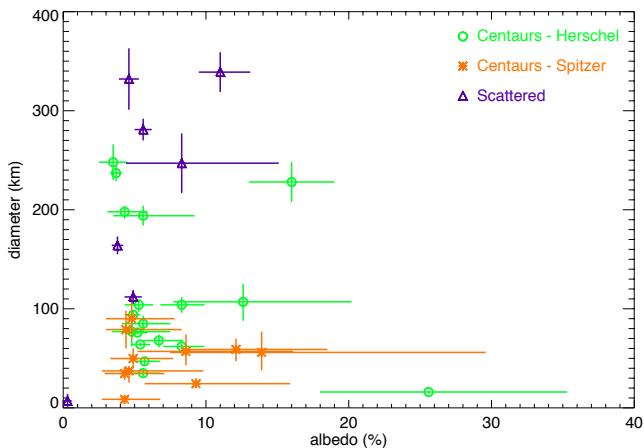


Fig. 4. Diameter versus albedo plot. We can see the gap in size between 120 to 190 km for the Centaurs. Objects with an albedo higher than 15% are suspected to be active. 2007 OR₁₀ is not included because its diameter ($D=1280$ km) is beyond the scale.

the sample of SDOs because they reside on larger orbits, making it very difficult to detect or observe the smaller objects in that population. This selection bias can be seen in Fig. 4, where there is only one SDO smaller than 120 km (2002 PN₃₄).

Stansberry et al. (2008) showed a tentative correlation (at 2.7σ) between albedo and semi-major axis for Centaurs, with all the objects at a < 20 AU having an albedo $< 5\%$. Our data do not show this correlation either for the Centaurs alone, or for the Centaurs plus SDOs (see Table 4). A tentative positive correlation between albedo and perihelion is also discussed in Stansberry et al. (2008), which would suggest that objects at lower perihelion have a lower albedo. Our results do not confirm this correlation in either the Centaur or Centaur plus SDOs samples (see Table 4).

Similarly, the correlation between p_V and $r(h)$ previously noticed by Stansberry et al. (2008) is not confirmed by our results, even when we include the SDOs (Figure 5, upper panel). There is no evidence for a correlation between albedo and inclination or eccentricity. All of this together seems to indicate that the albedo of Centaurs is not strongly influenced by their dynamical properties.

Santos-Sanz et al. (2012) reported positive correlations between D and $r(h)$ and between p_V and $r(h)$ for the SDOs. The correlation between D and $r(h)$ exists and is strong for our sample, too, but it is clearer when we consider both SDO and Centaurs. We note that the large objects ($D > 120$ km) have orbits with $8 < q < 35$ AU, while those with $D < 120$ km) are restricted to orbits with $5 < q < 20$ AU (see Fig. 6). The correlation D vs a is stronger when the SDOs are included. All of these effects probably result from discovery bias and our criteria for selecting the Herschel targets.

In the plot of albedo vs. spectral slope (fig. 7 top panel), we can clearly see the difference between gray (smaller slope) and red (larger slope) objects. There is no object with slopes from 18 to 28%/1000 Å, this is just a consequence of the color bimodality in the population. However, other patterns appear in the albedo vs. color representation with most of the gray objects being dark, while the red ones span a broader range of albedos. Even if there are some gray objects with high albedos that had not been included in previous studies, the 74% of the gray cluster (those with spectral slope $< 18\%$) have an albedo $< 6\%$, while all the

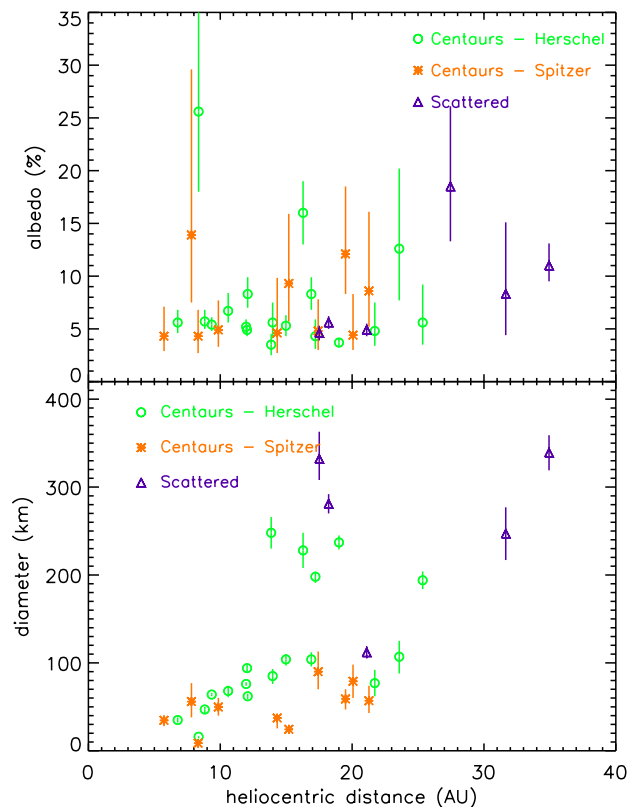


Fig. 5. Albedo and diameter versus heliocentric distances. The apparent correlation between heliocentric distance and diameter is probably an observational bias.

red objects have an albedo $> 5\%$, so most of the objects with low albedo are found in the gray group. The gray Centaurs seem to be more clustered in albedo, with a mean value of $5.73 \pm 3.6\%$ considering Chiron and 29P (the only two objects in this group with $p_V > 8\%$), and $4.8 \pm 1.3\%$ without them. For the redder objects the albedos can vary in a more continuous way from 5 to 14% with a mean value of 8.5%. To test a statistical significance of this result we ran a Kolmogorov-Smirnov test, our null hypothesis being that both samples are derived from the same distribution. We removed the gray Centaur Chiron from the sample, because it was active during the observation. We also discarded 2007 OR₁₀ since, as explained before, this red Centaur has a size, albedo, and surface composition very different from the rest of the sample. The KS test rules out the null hypothesis with a p -value of 0.1%, which means that the albedos of the red and gray groups of centaurs are not drawn from the same distribution.

Radiative transfer models show that mixtures of volatile ice and non-volatile organics might account for the extremely red surfaces of some TNOs and the red lobe of the Centaur population (Grundy 2009). For these red objects with lower perihelia, these materials could become progressively darker and less red as the ice sublimates away. However, reality is more complex and additional processes have to be considered. Cometary activity might trigger episodes of fast sublimation and the development of mantles of silicates, masking the original ices and darkening the surface. This is just what Melita & Licandro (2012) showed, all the objects in the gray lobe have passed a longer time in orbits with smaller perihelion. Accordingly, the albedo vs slope distribution of our sample is compatible with a red lobe

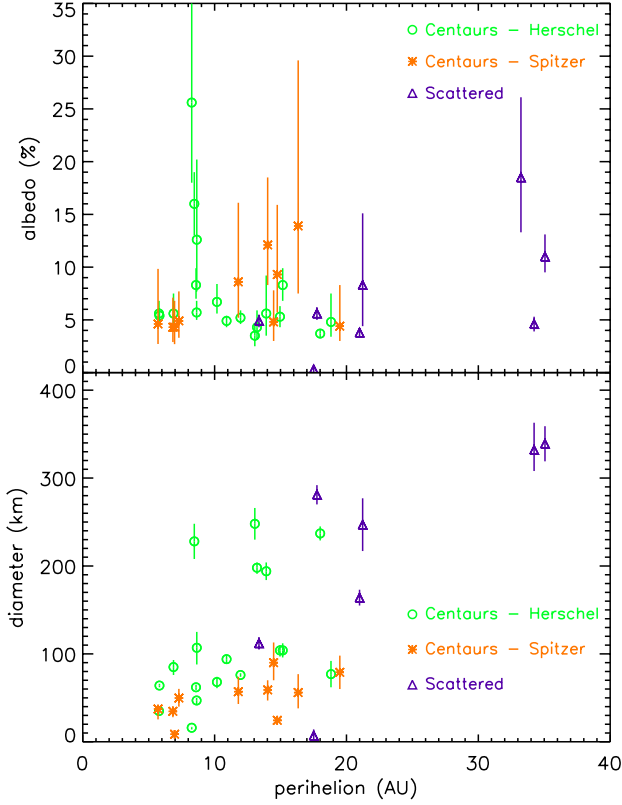


Fig. 6. Albedo and diameter versus perihelion distances.

of Centaurs richer in ices and organics with a higher albedo, and a gray lobe covered by surfaces poor in ice and rich in silicates with lower albedos affected by rapid sublimation typical of episodes of cometary activity. We can explain the objects in the gray group with higher albedo as being active Centaurs that may have some neutral-colored ices exposed on the surface as a result of that activity or a recent impact.

Another interesting result comes from the comparison of diameter vs slope. Again we can see the gap between $S^2=18$ and 28 that separates the gray and red lobe of the Centaurs. The lack of large objects in the red lobe is evident. All of our objects are smaller than 400 km in diameter (with the exception of 2007 OR₁₀ with 1280 km and the ability to retain volatiles), which means that all of them are too small to have retained part of the original inventory of volatiles on their surfaces. We can draw a horizontal line at 120 km so that all the objects above it appear in the gray lobe, while objects below this limit appear either in the red or in the gray lobe. It is known that objects smaller than 100-150 km are fragments of collisions suffered by larger objects; this suggests that collisions might be a factor that affects the different colors of small and large objects.

Peixinho et al. (2012) found that the bimodal color distribution of Centaurs is a size-related phenomenon, common to both Centaurs and small KBOs, that is, independent of dynamical classification. We analyzed the smallest object sample and no strong correlations are present when we consider only the smaller Centaurs.

A low-significance 2.2σ medium correlation between albedo and spectral slope is, nonetheless, detected.

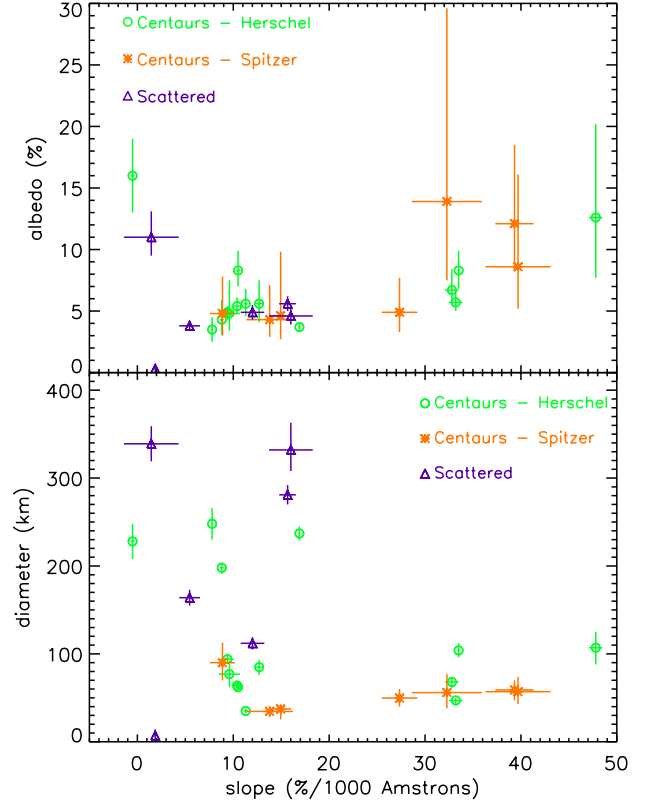


Fig. 7. Albedo and diameters versus visible spectral slopes. We can clearly see the gap in the slopes separating the gray and red objects. No red object larger than 120 km is present in the sample.

8. Discussion

Centaurs are smaller than most of the observed TNOs, and some of them were active recently or are currently active. This cometary activity can result in inhomogeneous surfaces, where two, or more different terrains are possible. In the near future, thermo-physical models should be applied in the Centaur population. Stellar occultation data are also valuable and can constrain diameters and albedos.

While Santos-Sanz et al. (2012) found a correlation between albedo and diameter in a sample of SDOs, one of the main results here is the absence of an albedo/diameter correlation in a larger sample. We analyzed here only a limited sample of Centaurs, only those with a radiometric diameter/albedo determination. But other analysis can be made using the H magnitude as a simile of diameter and assuming an albedo (Peixinho et al. 2012). Care must be taken in choosing the albedo to transform H magnitude to diameters. Here we show that for the larger Centaurs, the mean albedo is 4.2% (four objects, with the exception of the active Chiron), while the smaller Centaurs have a larger dispersion on albedo, from 4% to 15% (with the exception of 2005 UJ₄₃₈).

Our results show an excellent concordance with those of Bauer et al. (2013) in both diameters and albedos. However, our errors are smaller which results in a more precise estimate for individual objects. The error in the mean of any variable is the standard deviation. Objects whose differences are not within the error bar can be explained by a combination of different effects: a different value of the absolute magnitude, the lack of observa-

tions on some of the bands, or the different observing conditions. Our results are also equivalent within the 1σ error bar when we studied the mean albedo of the population. Bauer et al. (2013) found a mean albedo of $8\pm 4\%$ while we found a similar value of $6.9\pm 4.8\%$ for the Centaurs and a $6.7\pm 4.8\%$ for the whole sample. Another interesting result is the difference in albedos within the Centaur population. The mean albedos of our red and gray objects are $8.5\pm 4.9\%$ and $5.6\pm 1.2\%$, respectively. A similar result was also observed by Bauer et al. (2013), with a mean albedo of $12\pm 5\%$ for the redder objects and of $6\pm 2\%$ for the gray ones. Our results also show that the size distribution of the Centaurs in both groups is different, there are no large objects in the red lobe.

For the origin of the Centaurs we can add that the Centaur region is being resupplied, but the exact source region is unknown. They may be coming from the dynamical class of scattered-disk TNOs or from an yet unknown source (Volk & Malhotra 2008), for example as from the inner Oort cloud (Emel'yanenko et al. 2005), and there may be an exchange between the Centaur region and the Trojans of Jupiter and Neptune. Comparing the color distribution of Jupiter Trojans with those of other bodies, Fornasier et al. (2007) found that the Jupiter Trojans and neutral/gray Centaurs have fairly similar mean colors, but different color distributions. If there are several source regions, what is the contribution from each of them?

di Sisto et al. (2009) found that the vast majority of escaped Plutinos have encounters with Neptune and that this planet governs their dynamical evolution. When a Plutino escapes from the resonance, it is transferred to either the scattered-disk zone ($q > 30$ AU) or the Centaur zone ($q < 30$ AU), but eventually switches from Centaurs to SDOs or vice versa because of the dynamical influence of Neptune. The escaped Plutinos would have a mean lifetime in the Centaur zone of 108 Myr and their contribution to the Centaur population would be somewhat smaller than 6% of the total Centaur population. In this way, escaped Plutinos would be a secondary source of Centaurs. This is consistent with the findings of Mommert et al. (2012), who found no correlation between the diameters and albedos of Plutinos.

Some Centaurs (10%) show comet-like activity even though they are far away from the Sun. At distances outside the water zone, that is 5-6 AU, such activity cannot be explained by direct water-ice sublimation alone (Meech & Svoren 2004). This suggests that mass loss is driven by a process other than the sublimation of water ice. There have been some attempts to explain this by the crystallization of amorphous ice via the release of trapped gas (Capria et al. (2000); Notesco et al. (2003)), or CO₂ ice (Jewitt 2009). On the other hand, some Centaurs remain inactive even though their perihelia are small.

One scenario could be that the entire Centaur population is a mixture from different sources: Jupiter Trojans, Plutinos, SDOs, and the inner Oort cloud. Moreover, we are ignorant of the size of the object that became a Centaur. Smaller objects might be injected from the original source or be pieces of larger objects that were disrupted. This agrees with Peixinho et al. (2012) who found that both small Centaurs and small TNOs have a color bimodality.

In some respects the Centaurs resemble the near Earth objects (NEOs) of the trans-Neptunian region. Like the NEOs, they are dynamically unstable and short-lived, and they are thought to sample different populations of the TN belt. Given their diverse sources, why look for correlations between their properties at all? One reason is that this is a test of the idea that they are drawn from diverse parent populations: discovering a strong correlation in the Centaurs that would match a correlation

in another TNO population would call that hypothesis into question. Another reason is that individual Centaurs experience a different thermal evolution, because their orbital parameters, and their physical characteristics might provide clues about the nature of that evolution. As Melita & Licandro (2012) showed, gray/red colors are related with the time the objects spent near the Sun and are not related with the actual perihelion distance. Thermal evolution (de-volatilization) of Centaurs might also lead to measurable changes in their size. This might be an interesting area for future modeling, and might provide new insight into the sizes we present here.

9. Summary and conclusions

Our main findings are summarized as follows:

- We presented 16 diameters and albedos (and the beaming factors where possible) of Centaurs observed with Herschel-PACS. We merged our results with 12 other radiometric results from the literature to statistically analyze the distribution of sizes and albedos. We also used the albedos and diameters of eight SDOs obtained with Herschel. The final sample consisted of 28 Centaurs and 8 SDOs.
- Most of the Centaurs in our sample are small objects (82% are smaller than 120km) and the distribution of sizes is bimodal with a lack of objects with sizes between 120 and 190 km.
- Most of the Centaurs in our sample are low-albedo objects (61% have a $p_v < 6\%$), the remaining objects show an albedo between 6 and 16% (with the exception of 2005 UJ₄₃₈).
- There is no correlation between diameter and albedo. The mean albedo for our small and large Centaurs is $7.0\pm 4.0\%$ and $6.2\pm 5.0\%$, respectively.
- The albedo of the Centaurs is not correlated with their orbital parameters. No correlation is found between the albedo and the orbital parameters (a,e,i,q) and r(h). The same is true for the diameter we found no correlation.
- When we compared albedo and diameter with the surface properties (spectral slope) we clearly saw the typical bimodal distribution, with a gray lobe formed by objects with $S' < 18\%$ and a mean albedo of 5.6%; and a red lobe formed by those with a spectral slope larger than 28% and a mean albedo of 8.5%. Moreover, the color distribution of the small and large objects is different. Our data clearly showed that all the large Centaurs are gray, while the small ones can be found in either the red or gray group. Color bimodality is only present in small Centaurs.

Acknowledgements. RD acknowledges the support of MINECO for his Ramon y Cajal Contract. N.P.A.'s work was supported by MINECO through a fellowship of the Juan de la Cierva program. A.P. acknowledges grant LP2012-31. N.P.A. and P. S-S. acknowledge support by contract AYA2011-30106-C02-01. The work of C.K. has been supported by the Hungarian Space Office and the European Space Agency through contract PECS-98073, the K-104607 grant of the Hungarian Research Fund (OTKA), and the Bolyai Research Fellowship of the Hungarian Academy of Sciences. EV acknowledges the support of the German DLR project number 50 OR 1108. This work is based [in part] on observations made with the Spitzer Space Telescope, which is operated by the Jet Propulsion Laboratory, California Institute of Technology under a contract with NASA. NP acknowledges funding by the Gemini-Conicyt Fund, allocated to project N° 32120036.

References

- Andronico, G., Baratta, G. A., Spinella, F., & Strazzulla, G. 1987, *A&A*, 184, 333
- Barucci, M. A., Alvarez-Candal, A., Merlin, F., et al. 2011, *Icarus*, 214, 297

- Barucci, M. A., Belskaya, I. N., Fulchignoni, M., & Birlan, M. 2005, *AJ*, 130, 1291
- Barucci, M. A., Brown, M. E., Emery, J. P., & Merlin, F. 2008, *Composition and Surface Properties of Transneptunian Objects and Centaurs*, ed. M. A. Barucci, H. Boehnhardt, D. P. Cruikshank, A. Morbidelli, & R. Dotson, 143–160
- Bauer, J. M., Choi, Y.-J., Weissman, P. R., et al. 2008, *PASP*, 120, 393
- Bauer, J. M., Grav, T., Blauvelt, E., et al. 2013, *ApJ*, 773, 22
- Bauer, J. M., Meech, K. J., Fernández, Y. R., et al. 2003, *Icarus*, 166, 195
- Belskaya, I. N., Bagnulo, S., Barucci, M. A., et al. 2010, *Icarus*, 210, 472
- Belskaya, I. N., Barucci, M. A., & Shkuratov, Y. G. 2003, *Earth Moon and Planets*, 92, 201
- Boehnhardt, H., Tozzi, G. P., Birkle, K., et al. 2001, *A&A*, 378, 653
- Braga-Ribas, F., Sicardy, B., Ortiz, J. L., et al. 2013, *ApJ*, 773, 26
- Brown, M. E., Burgasser, A. J., & Fraser, W. C. 2011, *ApJ*, 738, L26
- Brucker, M., Romanishin, W. J., Tegler, S. C., et al. 2008, in *Bulletin of the American Astronomical Society*, Vol. 40, AAS/Division for Planetary Sciences Meeting Abstracts #40, 483
- Brucker, M. J., Grundy, W. M., Stansberry, J. A., et al. 2009, *Icarus*, 201, 284
- Buie, M. W. & Bus, S. J. 1992, *Icarus*, 100, 288
- Bus, S. J., Bowell, E., & French, L. M. 1988, *IAU Circ.*, 4684, 2
- Bus, S. J., Bowell, E., Harris, A. W., & Hewitt, A. V. 1989, *Icarus*, 77, 223
- Campins, H., Telesco, C. M., Osip, D. J., et al. 1994, *AJ*, 108, 2318
- Capria, M. T., Coradini, A., De Sanctis, M. C., & Orosei, R. 2000, *A&A*, 357, 359
- Cruikshank, D. P., Imanaka, H., & Dalle Ore, C. M. 2005, *Advances in Space Research*, 36, 178
- Delsanti, A. C., Boehnhardt, H., Barrera, L., et al. 2001, *A&A*, 380, 347
- DeMeo, F. E., Fornasier, S., Barucci, M. A., et al. 2009, *A&A*, 493, 283
- Di Sisto, R. P. & Brunini, A. 2007, *Icarus*, 190, 224
- di Sisto, R. P., Fernández, J. A., & Brunini, A. 2009, *Icarus*, 203, 140
- Doressoundiram, A., Barucci, M. A., Tozzi, G. P., et al. 2005, *Planet. Space Sci.*, 53, 1501
- Doressoundiram, A., Peixinho, N., de Bergh, C., et al. 2002, *AJ*, 124, 2279
- Dotto, E., Barucci, M. A., Leyrat, C., et al. 2003, *Icarus*, 164, 122
- Dotto, E., Perna, D., Barucci, M. A., et al. 2008, *A&A*, 490, 829
- Duffard, R., Lazzaro, D., Pinto, S., et al. 2002, *Icarus*, 160, 44
- Emel'yanenko, V. V., Asher, D. J., & Bailey, M. E. 2005, *MNRAS*, 361, 1345
- Fernández, Y. R., Jewitt, D. C., & Sheppard, S. S. 2002, *AJ*, 123, 1050
- Fornasier, S., Barucci, M. A., de Bergh, C., et al. 2009, *A&A*, 508, 457
- Fornasier, S., Doressoundiram, A., Tozzi, G. P., et al. 2004, *A&A*, 421, 353
- Fornasier, S., Dotto, E., Hainaut, O., et al. 2007, *Icarus*, 190, 622
- Fornasier, S., Lellouch, E., Müller, T., et al. 2013, *A&A*, 555, A15
- Foster, M. J., Green, S. F., McBride, N., & Davies, J. K. 1999, *Icarus*, 141, 408
- Fraser, W. C. & Brown, M. E. 2012, *ApJ*, 749, 33
- Fulchignoni, M., Belskaya, I., Barucci, M. A., de Sanctis, M. C., & Doressoundiram, A. 2008, *Transneptunian Object Taxonomy*, ed. M. A. Barucci, H. Boehnhardt, D. P. Cruikshank, A. Morbidelli, & R. Dotson, 181–192
- Gehrz, R. D., Roellig, T. L., Werner, M. W., et al. 2007, *Review of Scientific Instruments*, 78, 011302
- Gladman, B., Marsden, B. G., & Vanlaerhoven, C. 2008, *Nomenclature in the Outer Solar System*, ed. M. A. Barucci, H. Boehnhardt, D. P. Cruikshank, A. Morbidelli, & R. Dotson, 43–57
- Groussin, O., Lamy, P., & Jorda, L. 2004, *A&A*, 413, 1163
- Grundy, W. M. 2009, *Icarus*, 199, 560
- Grundy, W. M., Noll, K. S., Virtanen, J., et al. 2008, *Icarus*, 197, 260
- Guilbert, A., Alvarez-Candal, A., Merlin, F., et al. 2009, *Icarus*, 201, 272
- Guilbert-Lepoutre, A. 2012, *AJ*, 144, 97
- Hainaut, O. R., Boehnhardt, H., & Protopapa, S. 2012, *A&A*, 546, A115
- Harris, A. W. 1998, *Icarus*, 131, 291
- Hartmann, W. K., Tholen, D. J., Meech, K. J., & Cruikshank, D. P. 1990, *Icarus*, 83, 1
- Hoffmann, M., Fink, U., Grundy, W. M., & Hicks, M. 1992, in *Liege International Astrophysical Colloquia*, Vol. 30, Liege International Astrophysical Colloquia, ed. A. Brahic, J.-C. Gerard, & J. Surdej, 203
- Horner, J., Evans, N. W., & Bailey, M. E. 2004, *MNRAS*, 354, 798
- Horner, J. & Wyn Evans, N. 2006, *MNRAS*, 367, L20
- Jewitt, D. 2009, *AJ*, 137, 4296
- Jewitt, D. C. 2002, *AJ*, 123, 1039
- Kiss, C. and Mueller, T., Vilenius, E., Pal, A., et al. 2013, *Experimental Astronomy*, 999, 999
- Lagerros, J. S. V. 1996, *A&A*, 310, 1011
- Lamy, P. & Toth, I. 2009, *Icarus*, 201, 674
- Lebofsky, L. A., Sykes, M. V., Tedesco, E. F., et al. 1986, *Icarus*, 68, 239
- Lebofsky, L. A., Tholen, D. J., Rieke, G. H., & Lebofsky, M. J. 1984, *Icarus*, 60, 532
- Lellouch, E., Santos-Sanz, P., Lacerda, P., et al. 2013, *A&A*, 557, A60
- Levison, H. F. & Duncan, M. J. 1997, *Icarus*, 127, 13
- Licandro, J. & Pinilla-Alonso, N. 2005, *ApJ*, 630, L93
- Lim, T. L., Stansberry, J., Müller, T. G., et al. 2010, *A&A*, 518, L148
- Marcialis, R. L., Hubbard, W. B., Hill, R., et al. 1994, in *Bulletin of the American Astronomical Society*, Vol. 26, AAS/Division for Planetary Sciences Meeting Abstracts #26, 1153
- Meech, K. J. & Belton, M. J. S. 1989, *IAU Circ.*, 4770, 1
- Meech, K. J. & Svoren, J. 2004, *Using cometary activity to trace the physical and chemical evolution of cometary nuclei*, ed. G. W. Kronk, 317–335
- Melita, M. D. & Licandro, J. 2012, *A&A*, 539, A144
- Mommert, M., Harris, A. W., Kiss, C., et al. 2012, *A&A*, 541, A93
- Mueller, M., Stansberry, J., Mommert, M., & Grundy, W. 2012, in *AAS/Division for Planetary Sciences Meeting Abstracts*, Vol. 44, AAS/Division for Planetary Sciences Meeting Abstracts, 310
- Müller, T. G., Lellouch, E., Bönhardt, H., et al. 2009, *Earth Moon and Planets*, 105, 209
- Müller, T. G., Lellouch, E., Stansberry, J., et al. 2010, *A&A*, 518, L146
- Notesco, G., Bar-Nun, A., & Owen, T. 2003, *Icarus*, 162, 183
- Ortiz, J. L., Baumont, S., Gutiérrez, P. J., & Roos-Serote, M. 2002, *A&A*, 388, 661
- Ortiz, J. L., Gutiérrez, P. J., Casanova, V., & Sota, A. 2003, *A&A*, 407, 1149
- Ortiz, J. L., Gutiérrez, P. J., Santos-Sanz, P., Casanova, V., & Sota, A. 2006, *A&A*, 447, 1131
- Ortiz, J. L., Sicardy, B., Braga-Ribas, F., et al. 2012, *Nature*, 491, 566
- Peixinho, N., Boehnhardt, H., Belskaya, I., et al. 2004, *Icarus*, 170, 153
- Peixinho, N., Delsanti, A., Guilbert-Lepoutre, A., Gafeira, R., & Lacerda, P. 2012, *A&A*, 546, A86
- Peixinho, N., Doressoundiram, A., Delsanti, A., et al. 2003, *A&A*, 410, L29
- Perna, D., Barucci, M. A., Fornasier, S., et al. 2010, *A&A*, 510, A53
- Perna, E., Dotto, C., Barucci, M., Mazzotta, T., & Vilenius, P. 2013, *A&A*, 0, A00
- Pinilla-Alonso, N., Licandro, J., & Lorenzi, V. 2008, *A&A*, 489, 455
- Poglitsch, A., Waelkens, C., Geis, N., et al. 2010, *A&A*, 518, L2
- Rabinowitz, D. L., Schaefer, B. E., & Tourtellotte, S. W. 2007, *AJ*, 133, 26
- Rieke, G. H., Young, E. T., Engelbracht, C. W., et al. 2004, *ApJS*, 154, 25
- Romanishin, W. & Tegler, S. C. 2005, *Icarus*, 179, 523
- Romanishin, W., Tegler, S. C., Levine, J., & Butler, N. 1997, *AJ*, 113, 1893
- Rousselot, P. 2008, *A&A*, 480, 543
- Santos-Sanz, P., Lellouch, E., Fornasier, S., et al. 2012, *A&A*, 541, A92
- Santos-Sanz, P., Ortiz, J. L., Barrera, L., & Boehnhardt, H. 2009, *A&A*, 494, 693
- Sicardy, B., Ortiz, J. L., Assafin, M., et al. 2011, *Nature*, 478, 493
- Spearman, C. 1904, *The American Journal of Psychology*, 100, 441
- Spencer, J. R., Lebofsky, L. A., & Sykes, M. V. 1989, *Icarus*, 78, 337
- Stansberry, J., Grundy, W., Brown, M., et al. 2008, *Physical Properties of Kuiper Belt and Centaur Objects: Constraints from the Spitzer Space Telescope*, ed. M. A. Barucci, H. Boehnhardt, D. P. Cruikshank, A. Morbidelli, & R. Dotson, 161–179
- Stetson, P. B. 1987, *PASP*, 99, 191
- Sykes, M. V. & Walker, R. G. 1991, *Science*, 251, 777
- Tegler, S. C., Bauer, J. M., Romanishin, W., & Peixinho, N. 2008, *Colors of Centaurs*, ed. M. A. Barucci, H. Boehnhardt, D. P. Cruikshank, A. Morbidelli, & R. Dotson, 105–114
- Tegler, S. C., Romanishin, W., & Consolmagno, G. J. 2003, *ApJ*, 599, L49
- Thirouin, A., Ortiz, J. L., Duffard, R., et al. 2010, *A&A*, 522, A93
- Tholen, D. J., Hartmann, W. K., Cruikshank, D. P., et al. 1988, *IAU Circ.*, 4554, 2
- Tiscareno, M. S. & Malhotra, R. 2003, *AJ*, 126, 3122
- Veeder, G. J., Hanner, M. S., Matson, D. L., et al. 1989, *AJ*, 97, 1211
- Vilenius, E., Kiss, C., Mommert, M., et al. 2012, *A&A*, 541, A94
- Volk, K. & Malhotra, R. 2008, *ApJ*, 687, 714
- Werner, M. W., Roellig, T. L., Low, F. J., et al. 2004, *ApJS*, 154, 1
- Wright, E. L., Eisenhardt, P. R. M., Mainzer, A. K., et al. 2010, *AJ*, 140, 1868

Table 1. Centaur orbital and physical data. All orbital parameters are from the Minor Planet Center (MPC). The table lists the semi-major axis, the eccentricity, and the inclination of each Centaur as well as the rotational period in hours (errors are presented when available in literature) and light-curve amplitude in magnitudes. The last 3 columns are the taxonomic classification, the visible spectral slope and information on the surface composition (see the description of each Centaur in the text for references). Also in last column there is an indication if the object overlaps with the WISE sample, indicated with (Wise). This table also presents the data for Chiron and Chariklo published in Fornasier et al. (2013).

Herschel Centaurs										
Name	a	q	e	i	Rot. Period [hr]	LC Ampl.	Tax.	Spec. Slope %/1000 Å	Ices	
(95626) 2002 GZ ₃₂	22.99	18.00	0.217	15.030	5.80	0.08	BR	16.9±0.1	Water? (Wise)	
(250112) 2002 KY ₁₄	12.62	8.63	0.316	19.456	3.56	0.13	RR	33.2±0.7	Water? maybe (Wise)	
(120061) 2003 CO ₁	20.68	10.91	0.472	19.763	10	0.07 - 0.10	BR	9.4±0.6	Water? maybe (Wise)	
(136204) 2003 WL ₇	20.27	14.95	0.262	11.163	8.24	0.05	BB	...	(Wise)	
2005 RO ₄₃	29.00	13.93	0.520	35.415	
(145486) 2005 UJ ₄₃₈	17.70	8.26	0.533	3.783	8.32	0.13	RR, IR	...	(Wise)	
(248835) 2006 SX ₃₆₈	22.25	11.96	0.462	36.287	BR	...	(Wise)	
(281371) 2008 FC ₇₆	14.79	10.18	0.312	27.105	RR	32.8±0.7	no Water (Wise)	
(55576) Amycus	24.95	15.18	0.392	12.345	9.76	0.16	RR	33.5±0.1	Water (Wise)	
(8405) Asbolus	18.10	6.88	0.620	17.610	8.935	0.32 - 0.55	BR	12.7±0.4	no ice	
(54598) Bienor	16.56	13.24	0.201	20.731	9.14	0.34 - 0.75	BR	8.8±0.2	Water (Wise)	
(10199) Chariklo	15.74	13.06	0.170	23.400	...	<0.1	BR	7.8±0.1	Water (Wise)	
(2060) Chiron	13.67	8.49	0.379	6.927	5.918	0.04 - 0.09	BB	-0.5±0.2	Water (Wise)	
(60558) Echeclus	10.71	5.82	0.457	4.342	26.802	...	BR	10.4±0.6	any (Wise)	
(10370) Hylonome	24.96	18.85	0.245	4.150	...	<0.04	BR	9.6±1.1	...	
(52872) Okyrhoe	8.34	5.79	0.306	15.660	9.72	0.07 - 0.04	BR	11.3±0.2	Water, maybe. (Wise)	
(5145) Pholus	20.28	8.65	0.573	24.705	9.98	0.15 - 0.60	RR	47.8±0.7	Water, Methanol	
(32532) Thereus	10.67	8.58	0.196	20.329	8.335	0.18 - 0.38	BR	10.5±0.2	Water. (Wise)	
Spitzer un-published Centaurs										
(119315) 2001 SQ ₇₃	17.52	14.47	0.174	17.4	8.875±1.301	...	
(119976) 2002 VR ₁₃₀	24.11	14.75	0.388	3.5	
2004 QQ ₂₆	22.88	19.50	0.148	21.5	
2000 GM ₁₃₇	7.90	6.97	0.118	15.8	
Spitzer re-analyzed targets										
29P	6.00	50.73	0.042	9.37	288±24	14.94±1.09	(Wise)	
(7066) Nessus	24.48	11.80	0.518	15.6	39.7 ± 3.4	...	
(31824) Elatus	11.80	7.29	0.382	5.2	13.41 ± 0.04	0.102 ± 0.005	RR	27.34±1.86	Water. (Wise)	
(52975) Cyllarus	26.30	16.34	0.379	12.6	32.28±3.65	...	
(83982) Crantor	19.35	14.03	0.275	12.8	RR	39.22 ± 1.99	Water	
(63252) 2001 BL ₄₁	9.72	6.83	0.297	12.5	BR	13.8±2.42	None?	

Table 2. Individual observations of the sample of 16 Centaurs observed by Herschel-PACS and 4 Centaurs observed by Spitzer-MIPS. The results on these last 4 objects were not published before. The first line for each target contains the 4 subsequent measurements (twice the blue band, twice the green band, and four times the red band) for the first visit, the second line contains the measurements of the second visit, after the target has moved by a few beams. The identification number of the observation is given, followed by the duration and mid-time of the exposure. We also present the heliocentric distance (r), geocentric distance (Δ), and phase angle (α) of the observation.

Target	OBSIDs	Duration (sec.)	Mid-time	r (AU)	Δ (AU)	α ($^\circ$)
(95626) 2002 GZ ₃₂	1342202937-40	568	2010-08-12 17:19:21	19.006	19.232	3.0
	1342202967-70	568	2010-08-13 01:39:22			
(250112) 2002 KY ₁₄	1342211112-15	850	2010-12-13 16:37:30	8.824	8.547	6.2
	1342211144-47	850	2010-12-13 22:26:46			
(120061) 2003 CO ₁	1342202345-48	568	2010-08-09 18:23:36	12.032	11.842	4.8
	1342202361-64	568	2010-08-10 07:15:55			
(136204) 2003 WL ₇	1342191941-44	850	2010-03-10 01:03:04	14.980	15.217	3.7
	1342191966-69	850	2010-03-10 09:42:50			
2005 RO ₄₃	1342212848-51	850	2011-01-18 06:55:29	25.352	25.016	2.1
	1342213115-18	850	2011-01-19 07:03:23			
(145486) 2005 UJ ₄₃₈	1342218768-71	1414	2011-04-18 01:37:12	8.356	8.272	6.9
	1342218784-87	1414	2011-04-18 07:43:45			
(248835) 2006 SX ₃₆₈	1342196759-62	850	2010-05-20 13:14:29	11.961	12.246	4.6
	1342196771-74	850	2010-05-20 18:22:09			
(281371) 2008 FC ₇₆	1342222926-29	568	2011-06-22 08:34:29	10.599	10.574	5.5
	1342222933-36	568	2011-06-22 13:37:26			
Amycus	1342202341-44	850	2010-08-09 17:28:22	16.906	16.626	3.3
	1342202367-70	850	2010-08-10 08:38:51			
Asbolus	1342190921-24	548	2010-02-22 00:35:35	13.973	14.316	3.8
	1342190937-40	548	2010-02-22 06:40:11			
Bienor	1342213252-55	568	2011-01-24 12:52:20	17.216	17.553	3.0
	1342213274-77	568	2011-01-24 22:00:27			
Echeclus	1342201153-56	568	2010-07-23 18:09:47	9.353	9.008	6.0
	1342201194-97	568	2010-07-25 13:33:02			
Hylonome	1342215386-89	1132	2011-03-07 00:25:13	21.717	21.709	2.6
	1342215607-10	1132	2011-03-08 00:33:05			
Okyrhoe	1342202865-68	568	2010-08-11 17:49:38	6.771	7.044	8.1
	1342202893-96	568	2010-08-12 00:23:43			
Pholus	1342205148-51	850	2010-09-26 22:58:03	23.576	23.915	2.3
	1342205153-56	850	2010-09-27 08:15:50			
Thereus	1342216137-40	568	2011-03-06 03:09:48	12.082	12.190	4.7
	1342216150-53	568	2011-03-06 10:32:29			
Spitzer sample unpublished Centaurs						
Target	AORKEY	Duration (sec)	Mid-time	r (AU)	Δ (AU)	α ($^\circ$)
(119315) 2001 SQ ₇₃	26025216, 26029824	872	2009-03-24 10:14:21	17.427	17.354	3.3
(119976) 2002 VR ₁₃₀	26026752, 26031360	872	2009-03-25 07:23:28	15.199	14.982	3.7
2004 QQ ₂₆	26027520, 26032128	872	2009-03-24 05:45:20	20.070	20.030	2.8
2000 GM ₁₃₇	26026496, 26031104	872	2008-11-27 03:50:33	8.321	7.775	6.1

Table 3. Individual absolute magnitudes (H_{mag}) and Herschel flux densities (F_{70} , F_{100} and F_{160}), diameter (D), albedo (p_v), and beaming parameter (η) of the Centaur sample. Color-corrected Spitzer flux densities (F_{24} and F_{71}) of previously published targets and four unpublished targets. The object 29P is excluded from this table because we used the values published in Stansberry et al. (2008). All the used H_{mag} also consider the amplitude of the light-curve adding quadratically the 88% of half the amplitude to each uncertainty (when amplitude is unknown we assumed an amplitude of 0.2 mag -(Vilenius et al. 2012)-. For some of the objects this variation is significant, about 0.3-0.4 mag (e.g. Pholus and Asbolus). The MIPS and PACS data have been taken at very different epochs, hence have substantially different observing geometries.

Herschel sample									
Target	H_{mag} (mag)	F_{24} (mJy)	F_{71} (mJy)	F_{70} (mJy)	F_{100} (mJy)	F_{160} (mJy)	D (km)	p_v %	η
2002 GZ ₃₂	7.37 ± 0.10(a)	9.88 ± 0.31	44.49 ± 2.91	54.48 ± 1.80	41.16 ± 1.94	20.26 ± 2.17	237 ⁺⁸ ₋₈	3.7 ^{+0.4} _{-0.4}	0.97 ^{+0.05} _{-0.07}
2002 KY ₁₄	10.37 ± 0.07(b)	23.43 ± 1.20	14.81 ± 0.92	6.76 ± 1.29	47 ⁺³ ₋₄	5.7 ^{+1.1} _{-0.7}	1.20 ^{+0.35} _{-0.35}
2003 CO ₁	9.07 ± 0.05(c)	21.12 ± 0.68	34.02 ± 3.60	34.51 ± 1.45	23.73 ± 2.11	11.28 ± 1.63	94 ⁺⁵ ₋₅	4.9 ^{+0.5} _{-0.6}	1.23 ^{+0.12} _{-0.11}
2003 WL ₇	8.75 ± 0.16(d)	7.08 ± 0.21	20.95 ± 1.54	22.18 ± 1.30	15.07 ± 1.16	< 3.04	105 ⁺⁶ ₋₇	5.3 ^{+1.0} _{-1.0}	1.02 ^{+0.07} _{-0.05}
2005 RO ₄₃	7.34 ± 0.51(e)	0.81 ± 0.03	11.30 ± 0.93	12.69 ± 1.24	5.77 ± 2.48	194 ⁺¹⁰ ₋₁₀	5.6 ^{+3.6} _{-2.1}	1.12 ^{+0.05} _{-0.08}
2005 UJ ₄₃₈	11.14 ± 0.32(f)	8.05 ± 0.24	4.71 ± 0.96	5.02 ± 0.72	3.38 ± 0.89	2.78 ± 1.56	16 ⁺¹ ₋₂	25.6 ^{+9.7} _{-7.6}	0.34 ^{+0.09} _{-0.08}
2006 SX ₃₆₈	9.45 ± 0.11(g)	15.09 ± 0.48	26.65 ± 2.40	25.00 ± 1.12	15.63 ± 1.21	10.71 ± 1.94	76 ⁺² ₋₂	5.2 ^{+0.7} _{-0.6}	0.87 ^{+0.04} _{-0.06}
2008 FC ₇₆	9.44 ± 0.10(h)	26.79 ± 1.43	15.58 ± 1.72	5.00 ± 1.65	68 ⁺⁶ ₋₇	6.7 ^{+1.7} _{-1.1}	1.20 ^{+0.35} _{-0.35}
Amycus	8.27 ± 0.11(i)	6.19 ± 0.20	14.74 ± 1.93	17.02 ± 0.82	10.31 ± 0.91	6.53 ± 3.16	104 ⁺⁸ ₋₈	8.3 ^{+1.6} _{-1.5}	1.00 ^{+0.12} _{-0.13}
Asbolus(7)	9.13 ± 0.25(j)	73.52 ± 2.24	85.70 ± 9.56	8.51 ± 1.62	< 2.07	< 2.99	85 ⁺⁸ ₋₉	5.6 ^{+1.9} _{-1.5}	0.97 ^{+0.14} _{-0.18}
Bienor	7.57 ± 0.34(k)	3.51 ± 0.11	28.81 ± 4.77	37.51 ± 1.42	26.67 ± 1.36	14.45 ± 4.92	198 ⁺⁶ ₋₇	4.3 ^{+1.6} _{-1.2}	1.58 ^{+0.07} _{-0.07}
Echeclus(1)	9.78 ± 0.14(l)	4.91 ± 0.15	16.36 ± 4.86	42.15 ± 1.50	26.93 ± 2.17	16.55 ± 2.11	65 ⁺² ₋₂	5.3 ^{+0.7} _{-0.7}	0.87 ^{+0.04} _{-0.04}
Echeclus(2)	9.78 ± 0.14(l)	20.15 ± 0.61	42.15 ± 1.50	26.93 ± 2.17	16.55 ± 2.11	63 ⁺² ₋₂	5.5 ^{+0.9} _{-0.6}	0.81 ^{+0.04} _{-0.05}
Echeclus							64.6 ^{+1.6} _{-1.6}	5.2 ^{+0.70} _{-0.71}	0.86 ^{+0.036} _{-0.037}
Hylonome(3)	9.51 ± 0.08(m)	0.51 ± 0.08	< 4.798	2.76 ± 0.96	2.06 ± 1.09	4.06 ± 2.45	77 ⁺¹⁵ ₋₁₆	4.9 ^{+2.7} _{-1.7}	1.32 ^{+0.34} _{-0.32}
Hylonome(4)	9.51 ± 0.08(m)	0.44 ± 0.03	2.76 ± 0.96	2.06 ± 1.09	4.06 ± 2.45	77 ⁺¹⁷ ₋₁₅	4.7 ^{+2.8} _{-1.4}	1.35 ^{+0.31} _{-0.30}
Hylonome							74 ⁺¹⁶ ₋₁₆	5.1 ^{+3.0} _{-1.7}	1.29 ^{+0.31} _{-0.31}
Okyrhoe	11.07 ± 0.10(n)	28.89 ± 0.89	37.53 ± 5.07	30.34 ± 1.80	14.82 ± 2.50	10.02 ± 3.64	35 ⁺³ ₋₃	5.6 ^{+1.2} _{-1.0}	0.71 ^{+0.12} _{-0.13}
Pholus(5)	7.68 ± 0.28(o)	3.13 ± 0.13	15.63 ± 7.11	4.83 ± 0.99	3.21 ± 1.86	< 3.91	99 ⁺¹⁵ ₋₁₄	15.5 ^{+7.6} _{-4.9}	0.77 ^{+0.16} _{-0.16}
Pholus(6)	7.68 ± 0.28(o)	0.95 ± 0.10	< 5.220	4.83 ± 0.99	3.21 ± 1.86	< 3.91	119 ⁺¹⁸ ₋₁₉	11.0 ^{+5.7} _{-3.6}	1.48 ^{+0.30} _{-0.28}
Thereus(8)	9.40 ± 0.16(p)	23.60 ± 0.73	43.90 ± 5.44	17.39 ± 1.22	9.68 ± 1.08	4.46 ± 2.05	62 ⁺³ ₋₃	8.3 ^{+1.6} _{-1.3}	0.87 ^{+0.08} _{-0.08}
Spitzer sample re-analyzed targets									
Target	H_{mag} (mag)	F_{24} (mJy)	F_{71} (mJy)	F_{70} (mJy)	F_{100} (mJy)	F_{160} (mJy)	D (km)	p_v %	η
Nessus	9.51 ± 0.22 (s)	0.38 ± 0.09	57 ⁺¹⁷ ₋₁₄	8.6 ^{+7.5} _{-3.4}	1.20 ^{+0.35} _{-0.35}
Elatus/2004		8.59 ± 0.12	< 5.97			
Elatus/2005	10.40 ± 0.09 (t)	6.05 ± 0.20	10.68 ± 4.30	49.8 ^{+10.4} _{-9.8}	4.9 ^{+2.8} _{-1.6}	1.20 ^{+0.35} _{-0.35}
Cyllarus	9.02 ± 0.15 (v)	0.21 ± 0.11	56 ⁺²¹ ₋₁₈	13.9 ^{+15.7} _{-6.4}	1.20 ^{+0.35} _{-0.35}
2001 BL ₄₁	11.34 ± 0.21 (w)	4.90 ± 0.15	34.6 ^{+6.1} _{+6.6}	4.3 ^{+2.8} _{-1.4}	1.20 ^{+0.35} _{-0.35}
Crantor	9.03 ± 0.16 (w)	2.26 ± 0.08	< 6.31	59 ⁺¹¹ ₋₁₂	12.1 ^{+6.4} _{-3.8}	1.20 ^{+0.35} _{-0.35}
2001 SQ ₇₃	9.15 ± 0.11 (q)	1.81 ± 0.06	90 ⁺²³ ₋₂₀	4.8 ^{+3.0} _{-1.8}	1.20 ^{+0.35} _{-0.35}
2002 VR ₁₃₀	11.26 ± 0.39 (r)	0.27 ± 0.02	24.4 ^{+5.4} _{-4.6}	9.3 ^{+6.6} _{-3.6}	1.20 ^{+0.35} _{-0.35}
2004 QQ ₂₆	9.53 ± 0.36 (r)	0.63 ± 0.02	79 ± 19	4.4 ^{+3.9} _{-1.4}	1.20 ^{+0.35} _{-0.35}
2000 GM ₁₃₇	14.36 ± 0.38 (r)	0.75 ± 0.03	8.6 ± 1.5	4.3 ^{+2.6} _{-1.6}	1.20 ^{+0.35} _{-0.35}

References. (1) MIPS AORKEY 8808960 (2) MIPS AORKEY 26034432 (3) MIPS AORKEY 9038080 (4) MIPS AORKEY 12659968 (5) MIPS AORKEY 9040896 (6) MIPS AORKEY 12661760 (7) MIPS AORKEY 12660480 (8) MIPS AORKEY 9044480 (a) Rabinowitz et al. (2007); Romanishin & Tegler (2005); Doressoundiram et al. (2005); (b) Perna et al. (2010); (c) Perna et al. (2013); (d) Perna et al. (2013); (e) Herschel Database, Delsanti priv. communication 2013; (f) Perna et al. (2013); (g) Perna & Dotto (unpublished); (h) Perna et al. (2010) and Perna & Dotto (unpublished); (i) Perna et al. (2010); (j) Rabinowitz et al. (2007); Romanishin & Tegler (2005); (k) Rabinowitz et al. (2007); Romanishin & Tegler (2005); Doressoundiram et al. (2005); (l) Delsanti & Vilenius (priv. comm. 2013); (m) Romanishin & Tegler (2005); Doressoundiram et al. (2005); (n) Romanishin & Tegler (2005); Perna et al. (2010); Doressoundiram et al. (2005); (o) Romanishin & Tegler (2005); Perna et al. (2010); (p) Rabinowitz et al. (2007); Romanishin & Tegler (2005) (q) Tegler et al. (2003); Santos-Sanz et al. (2009); (r) from MPC R-band data (7–24 data points/target) using average V-R=0.57 ± 0.13 for Centaurs from MBOSS-2 Hainaut et al. (2012) and average $\beta = 0.09 ± 0.04$ from Perna et al. (2013); (s) Photometric data (N=1) from Romanishin et al. (1997) with new β_v fit from MPC/Steward observatory data (N=34); (t) Belskaya et al. (2003) and V-R color; (v) Tegler et al. (2003); Delsanti et al. (2001); Doressoundiram et al. (2002); Boehnhardt et al. (2001) new slope coefficient fit $\beta = 0.141 ± 0.073$; (w) Bauer et al. (2003); Tegler et al. (2003); Doressoundiram et al. (2005); Fornasier et al. (2004); DeMeo et al. (2009), default $\beta = 0.09 ± 0.04$; (w) Tegler et al. (2003), default $\beta = 0.09 ± 0.04$

Table 4. Correlation results on the different Centaur samples. Strongest correlations are listed in boldface.

Only Centaurs				
Variables	Number of data points	Correlation coefficient	Significance	Confidence level (σ)
D vs. p_V	28	$-0.21^{+0.27}_{-0.25}$	0.29	(1.06)
D vs. $Slope$	21	$-0.34^{+0.28}_{-0.23}$	0.14	(1.49)
D vs. a	28	$0.39^{+0.18}_{-0.22}$	0.04	(2.06)
D vs. e	28	$0.03^{+0.23}_{-0.23}$	0.86	(0.17)
D vs. i	28	$0.39^{+0.16}_{-0.19}$	0.04	(2.06)
D vs. q	28	$0.45^{+0.15}_{-0.19}$	0.02	(2.40)
D vs. Q	28	$0.34^{+0.19}_{-0.22}$	0.08	(1.76)
D vs. $r(h)$	28	$0.56^{+0.14}_{-0.17}$	<0.01	(3.11)
p_V vs. $Slope$	21	$0.38^{+0.27}_{-0.36}$	0.09	(1.71)
p_V vs. H_V	27	$0.03^{+0.27}_{-0.28}$	0.90	(0.13)
p_V vs. a	28	$0.14^{+0.22}_{-0.23}$	0.47	(0.73)
p_V vs. e	28	$0.32^{+0.20}_{-0.23}$	0.10	(1.66)
p_V vs. i	28	$-0.24^{+0.23}_{-0.21}$	0.23	(1.21)
p_V vs. q	28	$-0.01^{+0.24}_{-0.24}$	0.96	(0.04)
p_V vs. Q	28	$0.24^{+0.20}_{-0.22}$	0.22	(1.23)
p_V vs. $r(h)$	28	$0.07^{+0.25}_{-0.26}$	0.74	(0.34)
Centaurs + SDOs				
D vs. p_V	36	$-0.13^{+0.24}_{-0.23}$	0.45	(0.76)
D vs. $Slope$	27	$-0.32^{+0.20}_{-0.17}$	0.10	(1.65)
D vs. a	36	$0.64^{+0.11}_{-0.15}$	<0.01	(4.22)
D vs. e	36	$0.34^{+0.16}_{-0.18}$	0.04	(2.04)
D vs. i	36	$0.50^{+0.13}_{-0.15}$	<0.01	(3.13)
D vs. q	36	$0.66^{+0.10}_{-0.14}$	<0.01	(4.34)
D vs. Q	36	$0.61^{+0.12}_{-0.16}$	<0.01	(3.98)
D vs. $r(h)$	36	$0.72^{+0.09}_{-0.12}$	<0.01	(5.01)
p_V vs. $Slope$	27	$0.23^{+0.26}_{-0.29}$	0.26	(1.13)
p_V vs. H_V	35	$-0.01^{+0.22}_{-0.22}$	0.95	(0.06)
p_V vs. a	36	$0.02^{+0.20}_{-0.20}$	0.88	(0.14)
p_V vs. e	36	$0.11^{+0.21}_{-0.22}$	0.52	(0.65)
p_V vs. i	36	$-0.10^{+0.21}_{-0.20}$	0.57	(0.56)
p_V vs. q	36	$-0.02^{+0.21}_{-0.21}$	0.92	(0.10)
p_V vs. Q	36	$0.08^{+0.19}_{-0.19}$	0.66	(0.44)
p_V vs. $r(h)$	36	$0.07^{+0.21}_{-0.22}$	0.67	(0.42)
Centaurs smaller than 120 km				
D vs. p_V	23	$-0.11^{+0.31}_{-0.29}$	0.62	(0.49)
D vs. $Slope$	17	$-0.01^{+0.35}_{-0.34}$	0.97	(0.04)
D vs. a	23	$0.48^{+0.18}_{-0.23}$	0.02	(2.29)
D vs. e	23	$0.20^{+0.25}_{-0.27}$	0.37	(0.89)
D vs. i	23	$0.39^{+0.18}_{-0.21}$	0.06	(1.84)
D vs. q	23	$0.47^{+0.16}_{-0.20}$	0.02	(2.29)
D vs. Q	23	$0.43^{+0.19}_{-0.24}$	0.04	(2.06)
D vs. $r(h)$	23	$0.55^{+0.16}_{-0.21}$	0.01	(2.71)
p_V vs. $Slope$	17	$0.54^{+0.20}_{-0.30}$	0.02	(2.22)
p_V vs. H_V	22	$-0.15^{+0.32}_{-0.29}$	0.52	(0.65)
p_V vs. a	23	$0.26^{+0.25}_{-0.29}$	0.23	(1.20)
p_V vs. e	23	$0.22^{+0.26}_{-0.30}$	0.31	(1.01)
p_V vs. i	23	$-0.13^{+0.27}_{-0.25}$	0.56	(0.59)
p_V vs. q	23	$0.16^{+0.28}_{-0.31}$	0.46	(0.73)
p_V vs. Q	23	$0.32^{+0.23}_{-0.27}$	0.14	(1.47)
p_V vs. $r(h)$	23	$0.16^{+0.28}_{-0.31}$	0.48	(0.71)